THE ASTROPHYSICAL JOURNAL, 424:237–256, 1994 March 20

A MULTIWAVELENGTH STUDY OF STAR FORMATION IN THE L1495E CLOUD IN TAURUS

KAREN M. STROM[1] AND STEPHEN E. STROM[1]
Five College Astronomy Department, Graduate Research Center, 517-G, University of Massachusetts, Amherst, MA 01003;
e-mail: kstrom@hanksville.phast.umass.edu; sstrom@donald.phast.umass.edu
Received 1993 June 28; accepted 1993 September 27

ABSTRACT

We have carried out a deep (t = 30,000 s) X-ray search of the eastern portion of the L1495 cloud centered on the well-known weak line T Tauri star (WTTS) V410 Tau using the *ROSAT* PSPC. This deep exposure enabled a search for candidate pre–main-sequence (PMS) objects in this cloud to a limit ~20 times more sensitive than that typical of the fields examined with the *Einstein* searches. Despite assertions that the PMS population in Taurus-Auriga is nearly completely known, this X-ray survey revealed eight new PMS objects in a region 50′ in diameter, as compared to a previously known stellar population of 12 objects, including deeply embedded *IRAS* sources.

Spectroscopic and photometric observations enable us to place these objects in the H-R diagram. The newly discovered objects are predominantly stars of spectral-type M0 and later, and a large fraction (6/8) appear to be surrounded by circumstellar accretion disks as judged by their infrared excess and Hα emission. We combined the data for these X-ray-discovered objects with extant and new data for the previously identified PMS stars in this region to examine the history of star formation and the frequency distribution of stellar masses in this cloud.

If the "post-*ROSAT*" population is either complete or representative, we conclude (1) that star formation in L1495 East took place ~1×10^6 yr ago and that the spread in ages is small; (2) the frequency distribution of masses, $N(M)$, in this apparently coeval group appears to peak near log $M = -0.5$ (using masses derived from recently published PMS tracks of D'Antona & Mazzitelli and Swenson et al. and to decline toward lower masses. The derived $N(\log M)$ for L1495E compares well with the IMF derived from studies of stars in the solar neighborhood, a result which suggests that the Taurus-Auriga clouds are currently producing stars whose mass spectrum approximates the time/space-averaged IMF for the solar neighborhood.

Subject headings: circumstellar matter — ISM: individual (L1495) — stars: formation — stars: pre–main-sequence — X-rays: stars

1. INTRODUCTION

X-ray searches in regions of the recent star formation have proven efficacious not only in recovering previously known solar-type PMS objects (the classical T Tauri stars or CTTS), but in locating a class of objects of which few were previously identified, the weak-line T Tauri stars (WTTS) which lack the emission phenomena (Hα emission; metallic-line emission; optical excess (veiling) and infrared excess emission) which characterize CTTS. We report in this contribution the results of a deep search for X-ray sources in the vicinity of an actively star-forming cloud within the Taurus-Auriga cloud complex: L1495 E(ast). Our *ROSAT* PSPC image is the result of a total integration time of ~33,000 s and is centered on V410 Tau. We had originally hoped to use these data to search for periodic variations in X-ray flux from V410 Tau. However, the exposure did not span a large enough fraction of the 1.88 day rotation period to provide a definite result. The long effective integration time did permit a search for sources with X-ray luminosities as faint as 3.0×10^{38} ergs s^{-1} (unreddened), ~20 times deeper than any previous X-ray exposure in this region. As a result we located a number of additional candidate PMS stars (eight in number, compared to a previously identified PMS population of 12 objects in the same area). The goals of this study are (1) to locate optical counterparts for the newly identified sources; (2) to locate these objects in the HR Diagram using red spectra and optical and near infrared photometry; (3) to determine masses, ages and disk frequency for these objects; and (4) to construct an IMF for this population.

2. CLOUD ENVIRONMENT AND PREVIOUS STUDIES OF THE STELLAR POPULATION

Large-scale studies of the L1495 molecular cloud have been published by Duvert, Cernicharo, & Baudry (1986) and Fukui et al. (1992). These maps were made with radio telescopes of 2.5 m and 4 m diameter and therefore of relatively low spatial resolution ($\theta \sim 2'.5$). However, both maps show that the greatest concentration of molecular material is centered on the region containing V410 Tau, V892 Tau, DD Tau, and CZ Tau, the region upon which our *ROSAT* PSPC image is centered. Unfortunately, the region has not yet been studied either at high spatial resolution or in molecules sensitive to high densities (e.g., NH_3). Most molecular studies have been concentrated in the less-dense western part of this cloud. In view of the youth of this region and the degree of star-forming activity, it would be of great interest to pursue such studies.

Recent observations with the Nagoya University radio telescope, centered on known PMS objects show that the velocity dispersion as measured by line widths in this part of L1495 is larger than that seen in any other part of the Taurus-Auriga clouds, ≥ 3 km s^{-1}. The velocity dispersion drops considerably (to 1–1.5 km s^{-1}) in the outer parts of the cloud. In the western star-forming

[1] Visiting Astronomer, Kitt Peak National Observatory, National Optical Astronomy Observatory, which is operated by the Association of Universities for Research in Astronomy, Inc. (AURA), under cooperative agreement with the National Science Foundation.

center of L1495 (centered on V773 Tau) the velocity dispersion is ~ 2 km s^{-1}. Duvert et al. (1986) attributed the measured velocity dispersion to multiple components with a cloud collision possibly underway. However, while some of the line profiles appear to have weak additional components, the line profiles at cloud center appear to be smooth Gaussians with FWHM of ≥ 3 km s^{-1}. The mass of L1495E, within the region covered by the *ROSAT* PSPC image, lies between 180 $M_\odot$ as determined from the Nagoya C^{18}O map and 230 $M_\odot$ as determined from the ^{13}CO map (Ohnishi & Mizuno 1993).

Within a circle of 1° radius surrounding V410 Tau there are 19 known PMS objects; 12 of these lie within a circle of 25′ radius centered in the *ROSAT* field. There is one Herbig Ae/Be star, V892 Tau (Elias 1), centrally located in the cloud; also located in the central region are five WTTS, three CTTS, and three heavily embedded Class I sources (Lada 1987), one of which is known to drive a jet seen in Hα and [S II] (Strom et al. 1986; Goodrich 1993). In the outer region, $30' < r < 55'$, there are four CTTS and three WTTS. While M type stars are known among this population, they are all *early* M stars (spectral types M2 or earlier). This region of the Taurus clouds thus exhibits the spectral-type distribution characteristic of the rest of the Taurus clouds which show an apparent deficiency of late M stars, spectral types later than M2 (Cohen & Kuhi 1979), and therefore an apparent deficiency of stars with masses $M < 0.2\ M_\odot$.

3. OBSERVATIONS

The X-ray observation of the L1495E cloud was obtained in pointing mode with the *ROSAT* telescope using the position sensitive proportional counter (PSPC), between 4^h09^m on 1991 March 4 UT and 23^h25^m on 1991 August 2 UT. The total observation time over this period was 32,986 s. A description of the satellite, the telescope and the detector are given by Trümper (1983) and Pfeffermann et al. (1986). Because a portion of the data included in the standard analysis (SASS, version 5–6) contained observations taken during a period when the satellite was rolling (as indicated by the "housekeeping" data) the observation was rereduced excluding data taken during this period; the effective observation time is 25,757 s. The data were rereduced, excluding the portion affected by satellite roll, and analyzed using the PROS package (versions 2.1 and 2.2) under IRAF.[2]

The optical photometry at *R* and *I* was obtained on the night of 1992 December 11 UT with a Tektronix 2048 × 2048 CCD mounted in a universal CCD dewar on the Kitt Peak National Observatory 0.9 m telescope by Patrick Hartigan. The plate scale for the camera/telescope combination used for this observation was 0.″775 pixel^{-1}. A series of exposure times ranging from 10 s through 300 s was used for observations at *I* in order to obtain unsaturated images of the bright stars. A single exposure at *R* of 30 s duration was made. Only two stars suffered from saturated images in this exposure. Since the field was not crowded, the photometry was reduced using the DIGIPHOT package in IRAF using the new Landolt standard fields (Landolt 1992) and the PHOTCAL routine (Davis 1993).

The near-infrared photometry was obtained during four different runs due to the convolved effects of the small size of infrared arrays and the terrible weather in Arizona during the winter of 1993. The largest batch of near-infrared observations was taken by Ronald Probst on the night of 1993 January 12 UT using the SQIID photometer on the 1.3 m telescope at KPNO. Simultaneous images in *J*, *H*, and *K* were obtained using 256 × 256 PtSi arrays over a field of dimension 5.′4 × 5.′4; the size of each pixel is 1.″36. Each image is the sum of 2 "dithered" images, offset by $\sim 20''$ with an integration time of 180 s apiece. One additional field was obtained by Lynne Hillenbrand and the authors on 1992 December 27 UT, again with SQIID on the 1.3 m telescope at KPNO. The field centered on V892 Tau (Elias 1) was observed on 1992 January 27 UT with this same instrumentation by the authors. These data were all reduced using the SQIID package under IRAF. A few additional single-channel photometer measurements collected for other programs at San Pedro Martir are also included.

One additional field, as well as two previously observed fields, were observed by Michael Meyer and Patricia Knesek on 1993 March 11 UT at the 2.4 m Hiltner telescope at the MDM observatory on Kitt Peak using the NicMass camera (Skrutskie, Meyer, & Coutu 1994), equipped with a 256 × 256 HgCdTe NICMOS array having a field of dimension 4.′25 × 4.′25, and a plate scale of 0.″81 pixel. A series of four 3 s integrations in each filter was followed by a series of four 10 s integrations. These data were also reduced using the SQIID package under IRAF.

Spectra were obtained with HYDRA, the fiber-optic coupled spectrograph on the 4 m telescope at KPNO. We used the red fiber cable in conjunction with the BL 181 grating (316 l mm^{-1}) set at a central wavelength of 7600 Å, and a Tektronix 2048 × 2048 CCD to obtain spectra with a usable range from 5500 to 9200 Å; the effective resolution was 3 pixels or 6 Å. The spectra were then reduced using the DOHYDRA package within IRAF. Further analysis was done using the ONEDSPEC package. Spectral standards were established using the main-sequencer proper motion members of Praesepe (Jones & Stauffer 1991) for spectral types between F6 and M4. These standards were supplemented by the spectra of Kirkpatrick, Henry, & McCarthy (1991) for the late M stars.

4. IDENTIFICATION OF OPTICAL COUNTERPARTS TO *ROSAT* SOURCES

Our deep *ROSAT* PSPC exposure centered on V410 Tau allows us to assess the completeness of the known pre–main-sequence stellar population in this nearby active star formation region, of which only the periphery was observed with the *Einstein* satellite. The pre-*ROSAT* surveys do not provide the basis for evaluating the number of very low mass stars ($M \leq 0.3\ M_\odot$) in this region, leaving the question of the population of the low-mass end of the IMF unaddressed. Some information is provided by extant Hα surveys and the LkCa survey. This part of the Taurus clouds was covered by the Herbig, Vrba, & Rydgren (1986) survey for stars exhibiting Ca II H and K emission and three such stars (LkCa 4, 5, and 7) were found within the field of this *ROSAT* observation. These stars exhibit Hα emission and strong Li I λ6708 Å absorption (Strom et al. 1989a; Walter et al. 1988) and are clearly pre–main-sequence objects. However, their Hα emission equivalent widths are too small to allow detection by Hα objective prism

[2] IRAF is distributed by the National Optical Astronomy Observatories, which is operated by the Association of Universities for Research in Astronomy, Inc. (AURA), under cooperative agreement with the National Science Foundation.

surveys. Unfortunately, both the Hα and Ca II emission-line surveys reach only the brighter stars in the Taurus clouds ($R \leq 13$), and are incomplete for fainter stars, usually locating only those faint stars with unusually strong Hα emission.

Our deep *ROSAT* PSPC image of the V410 Tau region should enable a deep search for faint pre–main-sequence stars based on the elevated X-ray luminosity characteristic of PMS stars. Relative to main-sequence stars of the same spectral type, the X-ray luminosities of PMS stars may be 10^3 times greater (Feigelson 1986; Strom et al. 1990). Both CTTS and WTTS are strong X-ray emitters, with no significant difference in the X-ray properties of the two groups (Feigelson & Kriss; Strom et al. 1990; Gauvin & Strom 1992). Our observation should allow us to detect lightly obscured stars at the distance of the Taurus clouds (160 pc) having X-ray luminosities a factor of 20 lower than those found with the *Einstein* observations.

Unfortunately the sensitivity of a *ROSAT* PSPC observation is not uniform across the field. The point spread function of the *ROSAT* PSPC is a strong nonlinear function of the distance from field center, varying from FWHM $\sim 25''$ at field center to $1'$ at $\sim 30'$ from field center to $4'$ at the edge of the $2°$ field; therefore the sensitivity decreases rapidly outside the central $25'$ of the field. All but three (CK Tau 1, PSC 04154+2823, PSC 04158+2805) of the 12 previously identified pre–main-sequence stars (Herbig & Bell 1988) within the central field of radius $25'$ were easily detected. There is a faint extension on the X-ray image of Hubble 4 that may be attributable to CK Tau 1. In the outer annulus ($25' \leq r \leq 55'$) six more previously identified members (RY Tau, BP Tau, HDE 283572, FO Tau, LkCa 4, LkCa 7) of the Taurus cloud population are found. One of the previously known PMS stars, FO Tau, is not detected in this exposure. It is located at a distance $51'.8$ from the field center. While other PMS stars were detected at a distance from field center almost this great (notably RY Tau and HDE 283572 at $r = 46'.2$), the much lower luminosity of FO Tau apparently precludes its detection. In addition to the previously known members of the PMS population, eight additional X-ray detections ($>5\ \sigma$) appear in the central region of our exposure, which is centered on the densest part of the dark cloud. The positions of the previously known PMS stars are offset from the X-ray positions derived from the standard analysis by $\Delta\alpha = -3''.8 \pm 1''.0$ and $\Delta\delta = 8''.0 \pm 2''.5$. Using these offsets as a template, we were able to identify optical counterparts for each of the new X-ray sources on our deep *I*-band CCD frame. Within the positional error given by the local X-ray point spread function ($\Delta\theta \leq 10''$), six sources (V410 X-ray 1, 2, 3, 4, 6, and 7) appear to have unique optical counterparts while only two sources (V410 X-ray 5 and 8) within the central region of the field had more than one optical object as a possible identification. The object farthest from the field center (V410 X-ray 8, $r = 18'.5$) is located near the cloud periphery, hence complicating the identification owing to increasing contamination by background field stars. In this case we examined six possible identifications. Although most of these six candidates are much too far from the X-ray position, we felt that the possibility that the brightest star of the six, X-ray 8a, was the true X-ray source should be explored. The positional information for the sources detected in our *ROSAT* observation, as well as for the other PMS objects in the field, are presented in Table 1. The table gives the object name, the optical position, the X-ray position, the difference between the X-ray and optical positions in the sense of X-ray minus optical, and the radial distance from field center. A finding chart is given in Figure 1 (Plate 2).

4.1. *X-Ray Properties of the Sources*

For each detected X-ray photon, the time of arrival, position, and energy are recorded. This allows us to evaluate the variability of the source and to fit its spectral energy distribution with models which take into account both extinction from the intervening interstellar medium and the source temperature. Assuming that the X-ray emission from each of these sources arises in a stellar corona, we model the observed spectrum with a Raymond-Smith (Raymond & Smith 1977) thermal plasma, assuming solar abundances. We then solved for the temperature of the plasma and the column density of hydrogen atoms along the line of sight assuming the Morrison-McCammon (Morrison & McCammon 1983) interstellar X-ray absorption model. For the brighter X-ray sources, the signal to noise was sufficiently high to note strong systematic behavior in the fit residuals. Where appropriate, these sources were then refitted with a two-temperature model (Schrijver, Lemen, & Mewe 1989) where the line of sight extinction was held constant but two components of different temperature were included in the fit. These models provided substantially better fits (the χ^2 values were improved by factors of 5–35) to the X-ray spectra of the brighter sources. Single-component models were used for the fainter sources. The results of these fits for all stars are given in Table 2. Examples of the fits obtained for two high signal-to-noise sources (V410 Tau and Hubble 4) with different line-of-sight extinctions are shown in Figure 2. Also shown are the χ^2 plots in the temperature-log N_H plane. These plots demonstrate the sensitivity of the fits to line-of-sight extinction, even when the count rate is high. Using these fits, we are then able to calculate extinction corrected X-ray luminosities (0.2–2.4 keV) for these sources. When line-of-sight extinction is sufficiently high that few low-energy photons are detected, the error in the temperature determination increases, sometimes substantially. The two-temperature model serves only as an approximation to the more likely situation of a continuous temperature distribution. Therefore we feel that the presentation of formal error bars for the temperature and emission measure values would not be physically meaningful. Higher spectral resolution is necessary in order to make more physically meaningful measurements of the temperature distribution found in the region where the X-ray emission is formed. For sources with too few counts to yield a reliable fit, a model with $\log N_H = 21$ and $T = 1$ keV was fitted in order to allow an estimate of the X-ray luminosity.

We can compare the distribution of X-ray luminosities of the newly discovered X-ray objects with those of the previously identified PMS population of L1495E. The distributions of the two populations are shown in Figure 3. It is obvious that, while the *range* in X-ray luminosity for the two groups is similar, the *distributions* are vastly different. The median X-ray luminosity for the previously identified population is $\log L_x = 30.26$; the median X-ray luminosity for the newly identified population is $\log L_x = 29.00$. Therefore, by substantially increasing our sensitivity to low-luminosity sources, we have demonstrated that PMS stars may have X-ray luminosities at least as low as those found for Pleiades *main-sequence* stars of solar type (Stauffer et al. 1994).

While it was hoped that this observation would cover a full rotation period of V410 Tau, scheduling constraints led to the coverage of only about half of the period of this star. V410 Tau shows clear evidence of high-amplitude variation. We were unable to comment definitively on the relationship between the X-ray light curve and that seen in the optical. However, we are able to extract

PLATE 2

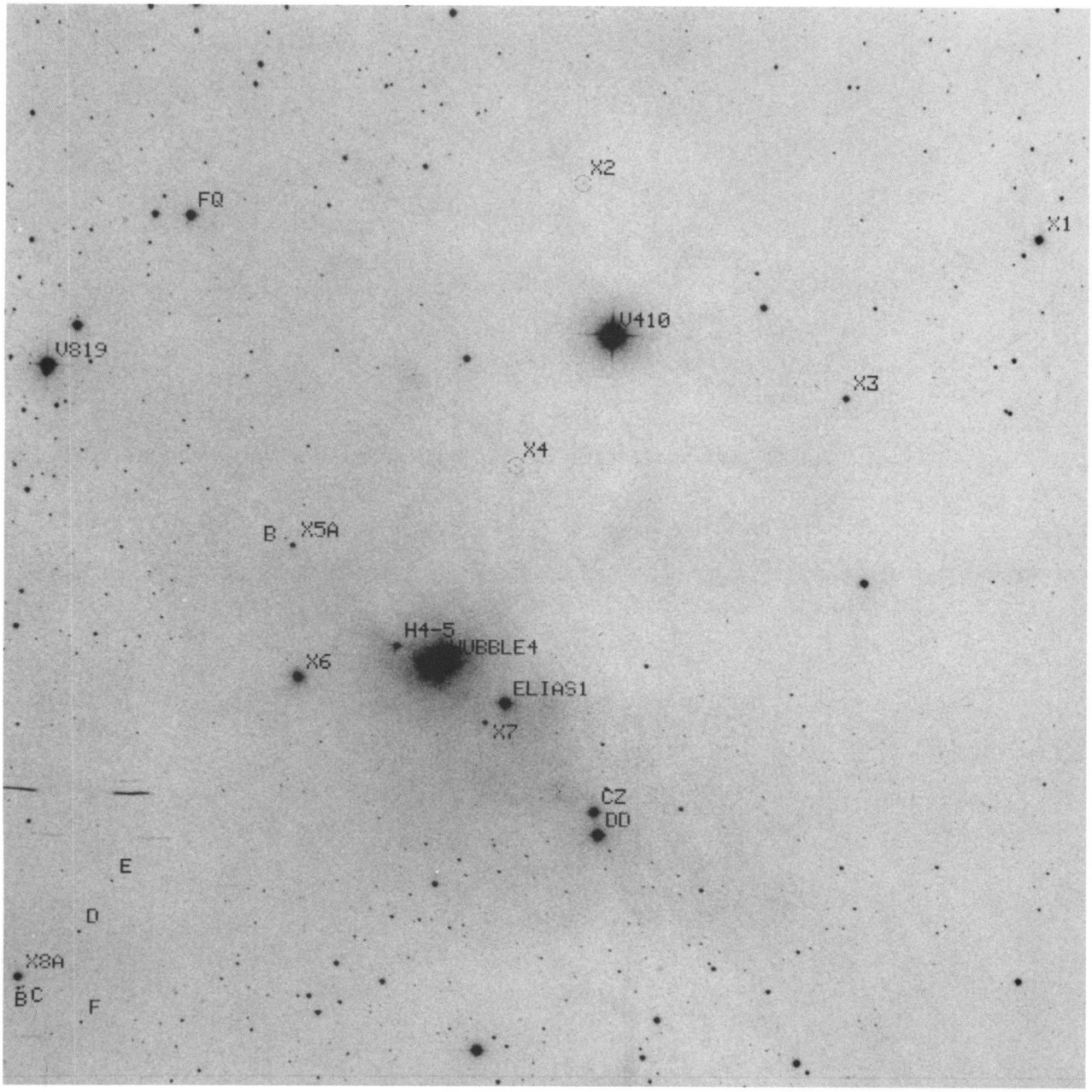

FIG. 1.—A finding chart for the X-ray–discovered PMS stars in the L1495E cloud. Also identified are the previously known PMS stars falling within the CCD frame. This image is 23'.5 on a side.

STROM & STROM (see 424, 239)

TABLE 1

X-RAY SOURCES AND OTHER PMS OBJECTS IN THE *ROSAT* FIELD

Object	Optical α(1950)	Optical δ(1950)	X-ray α(1950)	X-ray δ(1950)	$\Delta\alpha('')$	$\Delta\delta('')$	$r(')$	Alt. ID
FO Tau	4 11 43.60	28 05 02	...	...	...	...	51.8	PSC04117+2804
LkCa 4	4 13 22.42	28 00 13	4 13 22.0	28 00 24	-6	11	33.5	
CY Tau	4 14 27.67	28 13 29	4 14 27.6	28 13 46	-1	17	14.3	F04144+2813 [a]
LkCa 5	4 14 32.62	28 25 43	4 14 32.6	28 25 51	-1	8	12.7	
V410 x-ray 1	4 14 43.51	28 22 26	4 1 42.88	28 22 33	-8	7	9.6	B3 [b], K3-76 [c] F04147+2822 [a]
V410 x-ray 3	4 15 01.90	28 18 48	4 15 01.2	28 18 54	-10	6	5.3	
V410 Tau	4 15 24.83	28 20 02	4 15 24.6	28 20 10	-3	8	0.2	
DD Tau	4 15 25.10	28 09 14	4 15 24.9	28 09 25	-3	11	10.9	PSC04154+2809
CZ Tau	4 15 25.55	28 09 44	4 15 24.8	28 09 45	-9	1	10.8	
PSC04154+2823	4 15 25.79	28 24 01	...	...	...	...	3.8	K3-82 [c]
V410 x-ray 2	4 15 28.25	28 23 17	4 15 27.9	28 23 21	-4	4	3.7	
V410 x-ray 4	4 15 34.13	28 17 11	4 15 34.1	28 17 21	0	10	3.3	
V892 Tau	4 15 34.50	28 12 03	4 15 33.9	28 12 16	-8	13	8.7	Elias 1 PSC04155+2812
V410 x-ray 7	4 15 36.40	28 11 37	4 15 36.1	28 11 56	3	19	8.8	
Hubble 4	4 15 40.90	28 12 55	4 15 40.7	28 13 02	-3	7	8.1	
CK Tau 1	4 15 45.46	28 13 14	...	...	...	...	8.1	Hubble 4-5 [d] PSC04157+2813
PSC04158+2805	4 15 52.30	28 05 11	...	...	...	...	16.5	
V410 x-ray 6	4 15 55.10	28 12 30	4 15 54.7	28 12 37	-6	7	9.3	K3-89 [c]
V410 x-ray 5a	4 15 55.91	28 15 21	4 15 55.0	28 15 27	1	6	8.3	
V410 x-ray 5b	4 15 56.64	28 15 30			22	3		
FQ Tau	4 16 06.58	28 22 22	...	...	...	...	9.1	
BP Tau	4 16 08.61	28 59 15	4 16 09.8	28 59 13	-16	2	39.8	PSC04161+2859
V410 x-ray 8a	4 16 21.51	28 05 51	4 16 11.7	28 06 54	147	63	18.5	
V410 x-ray 8b	4 16 21.38	28 05 36			145	78		
V410 x-ray 8c	4 16 20.92	28 05 38			138	76		
V410 x-ray 8d	4 16 15.71	28 06 52			60	2		
V410 x-ray 8e	4 16 12.65	28 07 59			14	-65		
V410 x-ray 8f	4 16 15.23	28 04 52			53	122		
V819 Tau	4 16 19.92	28 19 03	4 16 19.2	28 19 13	-10	10	12.2	
LkCa 7	4 16 35.78	27 42 28	4 16 34.3	27 43 14	-19	46	40.7	
DE Tau	4 18 49.84	27 48 05	...	...	...	...	65.1	PSC04188+2748
RY Tau	4 18 50.85	28 19 35	4 18 51.0	28 18 24	-2	11	46.2	PSC04188+2819
HDE 283572	4 18 52.52	28 11 07	4 18 50.2	28 10 54	-32	13	46.2	

[a] Beichman, Boulanger & Moshir 1992.
[b] Briceño et al. 1993.
[c] Kim 1990.
[d] Strom et al. 1986.

variability data for each of our detected objects on shorter timescales because the arrival time of each detected photon is recorded as part of the observation. The Kolgomorov-Smirnov and Cramer–von Mises tests for constancy were performed on the time-sorted event files for the brighter sources in this field. Nine of the 12 sources bright enough to yield reliable results demonstrate clear variability. These results are also tabulated in Table 2, where we list the probability of variability found for the sources examined as well as the ratio of the maximum count rate to the minimum count rate seen in an 860 s bin. The large number of X-ray variables is not surprising in light of the extreme variability already noted for some of the PMS sources in the *Einstein* observations (Montmerle et al. 1983; Feigelson & DeCampli 1981). None of the eight newly discovered X-ray sources in L1495E was sufficiently bright to enable reliable variability indications.

At least one, and possibly two, X-ray flares occurred on PMS stars within the field during the observation period (Fig. 4). DD Tau clearly flared during the second half of the observation period following a long period of very low X-ray flux. Unfortunately, owing to a gap in the observation, we are unable to determine the rise time of the flare. The emission at the peak of the flare was a factor of 15 higher than that seen prior to the flare. The *e*-folding time for the decay of the flare is $\sim$1 hr; however, the star remained a factor of two above the flux level of its previous quiescent stage more than 5 hr after the flare began, at the end of the observation. It is possible that a less extreme event was seen on HDE 283572. Here the rise time is $\sim$1.4 hr, and the decay time is $\sim$6 hr. The peak flux is $\sim$6 times the pre-event flux. Another interpretation of the HDE 283572 observation would be that we are seeing variability associated with the rotation of an active region on the surface of the star. The rotation period of this star is $\sim$37 hr ($1^d.55$) (Walter et al. 1988); therefore our observation covered 0.65 periods. Lacking more data, we are unable to determine which interpretation is more likely.

TABLE 2

X-RAY SOURCE PARAMETERS

Object	Total Counts	$logN_H$	T_1 keV	EM_1	T_2 keV	EM_2	L_x $ergs/s$	Var. Prob.	Var. Ampl.
LkCa 4	1520	20.5 ± 0.4	1.30	10.23	0.27	9.98	2.4×10^{30}	> 99%	5
CY Tau	78	20.7 ± 0.6	1.71	9.12	...	...	1.5×10^{29}	...	...
LkCa 5	271	< 19.5	0.72	9.26	...	...	2.6×10^{29}	< 90%	...
V410 x-ray 1	209	20.6 ± 0.8	1.14	9.77	...	...	3.8×10^{28}	...	...
V410 x-ray 3	209	20.7 ± 0.6	1.13	9.78	...	...	3.8×10^{29}	...	...
V410 Tau	7338	20.4 ± 0.1	1.51	11.29	0.32	10.65	1.3×10^{31}	> 99%	2
DD Tau (flare)	252	21.2 ± 0.2	1.37	10.49	0.80	9.80	2.3×10^{30}	> 99%	15
DD Tau (pre-flare)	84	21.2	0.63	8.80	...	...	1.3×10^{29}	...	...
CZ Tau	76	< 20	0.71	9.06	...	...	7.4×10^{28}	...	...
V410 x-ray 2	153	21.7 ± 0.5	...	...	...	...	6.5×10^{29}	...	...
V410 x-ray 4	48	...	...	...	...	...	6.2×10^{28}	...	...
V892 Tau	446	22.1 ± 0.2	1.20	10.88	0.55	10.68	1.0×10^{31}	< 90%	...
V410 x-ray 7	146	22.1 ± 0.2	0.97	10.64	0.79	9.98	5.1×10^{30}	< 90%	...
Hubble 4	1496	21.5 ± 0.1	1.52	10.91	0.35	10.65	6.9×10^{30}	> 99%	2
V410 x-ray 6	55	...	...	...	...	...	4.0×10^{28}	...	...
V410 x-ray 5	62	< 22	...	...	...	...	1.3×10^{29}	...	...
FQ Tau	...	...	...	...	...	...	$< 2.7 \times 10^{28}$	...	...
BP Tau	2162	20.5 ± 0.5	1.22	10.16	0.20	9.72	1.8×10^{30}	> 99%	2
V410 x-ray 8	47	< 22	...	...	...	...	4.1×10^{28}	...	...
V819 Tau	1638	21.3 ± 0.3	1.14	10.73	0.25	10.62	7.7×10^{30}	> 90%	2
LkCa 7	4078	20.7 ± 0.3	1.79	10.83	0.35	10.13	5.6×10^{30}	> 99%	3
RY Tau	969	22.0 ± 0.1	1.22	11.36	0.54	10.66	2.8×10^{31}	> 99%	3
HDE 283572	2667	21.6 ± 0.1	1.45	11.53	0.44	11.30	5.8×10^{31}	> 99%	6

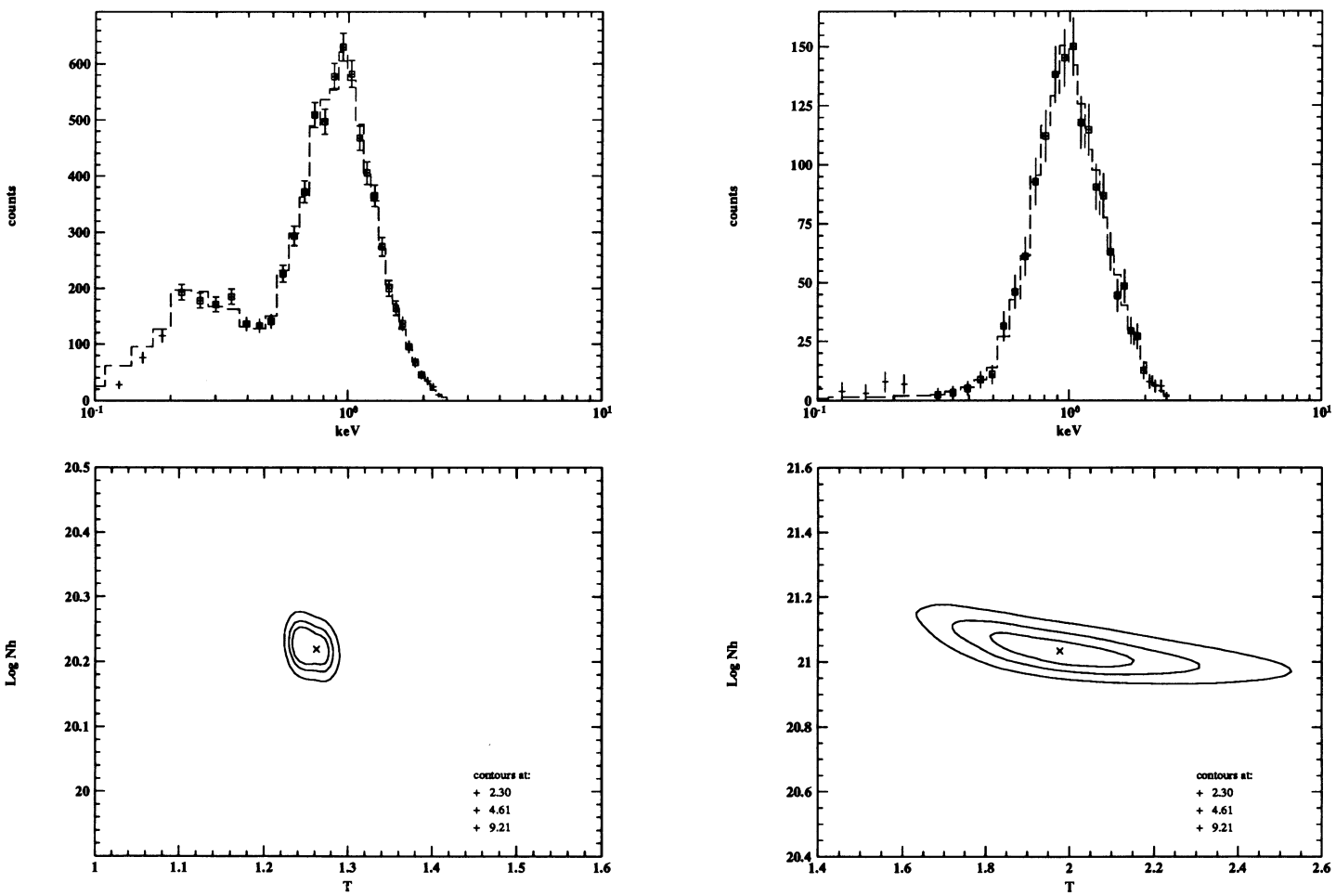

FIG. 2.—Examples of model X-ray spectrum fits to two high signal-to-noise observations. In the left-hand pair of plots is shown the fit to the X-ray spectrum of V410 Tau, a very lightly reddened object on the front surface of the cloud. In this case both the temperature (in keV) and the column of neutral hydrogen are well constrained as seen from the χ^2 plot on the lower left. In the other case (Hubble 4), the softer X-rays have been absorbed by the intervening cloud material. The lack of information at these energies leaves us with a fit that constrains the amount of intervening material but imposes less constraint on the temperature.

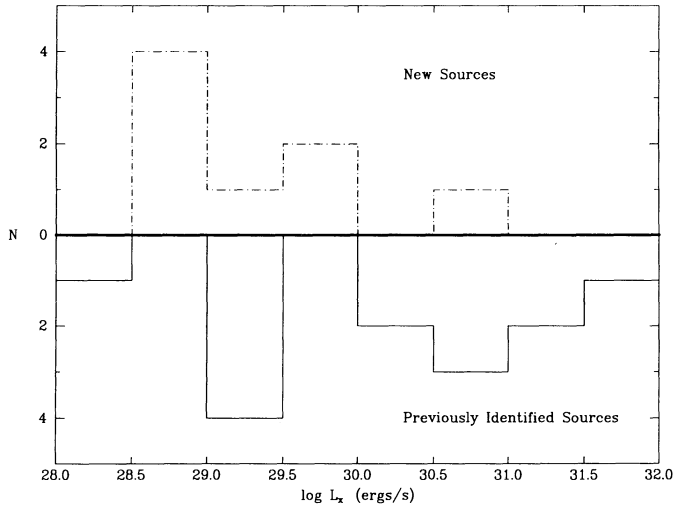

FIG. 3.—The distribution of X-ray luminosities for the previously identified members of the L1495E population compared with the X-ray luminosity distribution of the newly identified cloud population.

5. THE OPTICAL AND NEAR-INFRARED PHOTOMETRY AND SPECTROSCOPY FOR THE CANDIDATE OBJECTS

We have obtained new Cousins *R*- and *I*-band CCD observations of the central region of the *ROSAT* field, as well as new near-infrared (*J*, *H*, and *K*) observations of the X-ray sources in the same region. These data are presented in Table 3. When multiple observations have been made, the epoch is also given.

We were also able to obtain classification spectra in the red region for most of the possible X-ray source identifications (see Fig. 1) with the HYDRA fiber-optic fed spectrograph. Because of restrictions imposed by the placement of the optical fibers in the focal plane of the telescope, when a choice had to be made between two or more objects, the more likely identification (the brightest star nearest the X-ray position) was chosen. For this reason, no spectra were obtained of V410 X-ray 5b, V410 X-ray 8b and c. Although fibers were placed on V410 X-ray 2 and 4, no usable spectra were obtained owing to the faintness of the stars. No spectrum was obtained for DD Tau on this run. The spectral type for this star was taken from Hartigan, Strom, & Strom (1994). The spectral type for CZ Tau is a compromise since there is a definite change of spectral type with wavelength of at least two spectral subclasses, with later spectral types being found at longer wavelengths. This does not appear to be due to a variable veiling contribution, but is perhaps due to contamination of the spectrum with light from the subarcsecond companion found by Leinert et al. (1992).

Observations of the Praesepe main-sequence stars were used as spectral standards with which to classify our spectra of the X-ray sources in L1495E. The spectral types obtained are also given in Table 3; the spectral types should be good to one spectral subclass earlier that M2 and half a spectral subclass for stars later than M2. While the resolution of the spectra is too low to enable measurement of the strength of the Li λ6708 line, it was possible to measure the equivalent width of the Hα emission line, thus providing another criterion for including the star as a candidate member of the PMS population. These values are presented in Table 3 as well.

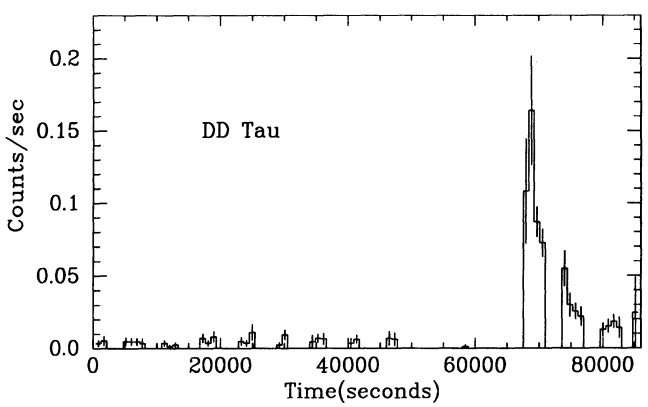

FIG. 4*a*

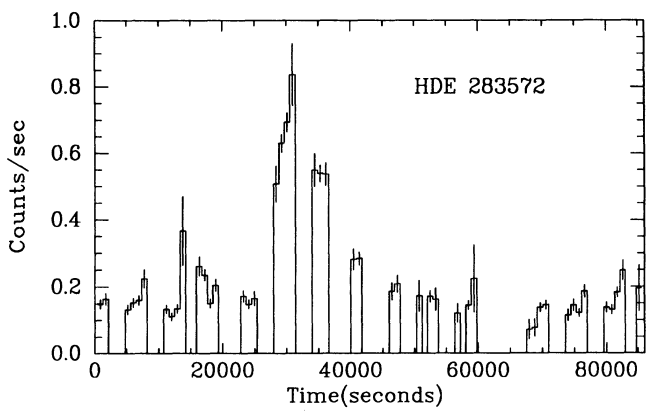

FIG. 4*b*

FIG. 4.—Plots of the X-ray count rate as a function of time from the beginning of the observation for (*a*) DD Tau and (*b*) for HDE 283572 binned in 860 s intervals. Both the low level of the flux prior to the flare and the high flare emission are obvious in DD Tau. Given the rotation period of HDE 283572 (134,000 s), it is less clear whether an event seen in the observation of this star is a small flare or is related to the rotation of an active region on the surface to the front face of the star.

TABLE 3

OPTICAL AND NEAR INFRARED DATA FOR THE *ROSAT* FIELD OBJECTS

Star	R	I	R-I	SpT	W($H\alpha$)	E_{RI}	A_v	J	H	K	J-H	H-K	Obs. Date
FO Tau	...	...	...	M2 [a]	117 [a]	...	1.94 [a]	9.70 [b]	8.77 [b]	8.19 [b]	0.93	0.58	
LkCa 4	11.54	10.56	1.02	K7	5	0.25	1.25	9.28	8.57	8.35	0.71	0.22	
CY Tau	12.38	11.20	1.18	M2	55	0.02	0.10	9.76	8.90	9.12	0.71	0.22	
LkCa 5	12.51	11.33	1.18	M2:	3.5	0.02	0.10	10.05	9.34	9.12	0.71	0.22	
V410 x-ray 1	14.15 ± 0.01	12.36 ± 0.01	1.79	M3.5-4	8	0.20	1.00	11.25 ± 0.04	10.01 ± 0.05	9.25 ± 0.04	1.24	0.76	1993 Jan 12
								10.13 ± 0.03	9.12 ± 0.04	8.77 ± 0.03	1.01	0.35	1993 March 11
V410 x-ray 3	15.80 ± 0.02	13.53 ± 0.01	2.27	M6	15	0.05	0.25	11.50 ± 0.04	10.93 ± 0.05	10.49 ± 0.04	0.57	0.44	1993 Jan 12
								12.08 ± 0.07	11.14 ± 0.04	10.77 ± 0.05	0.94	0.37	1993 March 11
V410 Tau	...	8.81 ± 0.01	...	K7	2.1	...	...	8.33	7.73	7.54	0.60	0.19	
	10.18	9.48	0.70			0.00	0.00						
DD Tau	12.63 ± 0.01	11.19 ± 0.01	1.44	M4 [c]	182	0.00	0.00	9.56	8.62	9.33	0.76	0.43	
CZ Tau	13.53 ± 0.01	11.80 ± 0.01	1.73	M3	5.6	0.36	1.80	9.90 ± 0.02	9.24 ± 0.02	8.77 ± 0.02	0.66	0.47	1992 Jan 27
PSC04154+2823	...	19.60 ± 0.21	...	...	...	...	...	15.00 ± 0.5	11.80 ± 0.05	10.13 ± 0.03	3.2:	1.67	1993 March 11
V410 x-ray 2	...	20.00 ± 0.50	...	...	...	...	...	13.86 ± 0.05	10.94 ± 0.04	9.43 ± 0.03	2.92	1.51	1993 March 11
V410 x-ray 4	...	19.30 ± 0.40	...	...	...	...	...	13.46 ± 0.10	11.07 ± 0.05	9.69 ± 0.04	2.39	1.38	1993 Jan 12
V892 Tau	13.14 ± 0.01	11.43 ± 0.01	1.71	B9	> 6.5	1.77	8.85	8.55 ± 0.02	6.91 ± 0.02	5.64 ± 0.02	1.64	1.27	1992 Jan 27
V410 x-ray 7	17.79 ± 0.10	15.17 ± 0.01	2.62	M1	5	1.60	7.90	11.88 ± 0.02	10.05 ± 0.02	9.16 ± 0.02	1.83	0.89	1992 Dec 27
Hubble 4	...	9.85 ± 0.01	...	K7	3.0	...	...	8.56 ± 0.02	7.68 ± 0.02	7.29 ± 0.02	0.88	0.39	1992 Jan 27
	11.92	10.65	1.27			0.50	2.45	8.52	7.61	7.26	0.91	0.35	
								8.66 ± 0.02	7.67 ± 0.02	7.29 ± 0.02	0.99	0.38	1988 Sept 28
CK Tau 1	16.40 ± 0.03	14.83 ± 0.01	1.58	M2:e	285	0.42	2.10	12.49 ± 0.03	11.35 ± 0.03	10.83 ± 0.02	1.14	0.52	1988 Sept 28
								12.53 ± 0.04	11.36 ± 0.02	10.80 ± 0.02	1.17	0.56	1992 Jan 27
								12.69 ± 0.03	11.26 ± 0.02	10.83 ± 0.02	1.43	0.43	1992 Dec 27
PSC04158+2805	17.11 ± 0.06	14.97 ± 0.01	2.14	...	>100 [d]	...	...	13.15[d]	11.92 [d]	10.80 [d]	1.12	1.23	
V410 x-ray 6	15.08 ± 0.01	13.00 ± 0.01	2.08	M5	9.2	0.17	0.83	10.54 ± 0.04	9.67 ± 0.05	9.05 ± 0.04	0.87	0.62	1992 Dec 27
V410 x-ray 5a[e]	17.14 ± 0.06	14.65 ± 0.01	2.49	M5	18	0.57	2.59	11.88 ± 0.04	10.80 ± 0.05	10.12 ± 0.04	1.08	0.68	1992 Dec 27
V410 x-ray 5b	...	18.42 ± 0.15	...	...	...	...	...	14.43 ± 0.10	13.47 ± 0.07	12.83 ± 0.05	0.96	0.64	1992 Dec 27
FQ Tau	13.49 ± 0.01	11.77 ± 0.01	1.72	M4	77	0.09	0.45	10.98 [b]	10.31 [b]	9.83 [b]	0.67	0.48	
BP Tau	11.23	10.39	0.84	K7	40	0.07	0.35	9.30	8.42	8.05	0.88	0.37	
V410 x-ray 8a	14.55 ± 0.01	12.65 ± 0.01	1.90	M0-2 III	5a	0.87	4.35	10.25 ± 0.04	8.85 ± 0.05	8.23 ± 0.04	1.40	0.62	1993 Jan 12
V410 x-ray 8b	18.14 ± 0.14	16.22 ± 0.02	1.92	...	...	...	...	13.82 ± 0.04	12.74 ± 0.05	11.96 ± 0.04	1.08	0.78	1993 Jan 12
V410 x-ray 8c	18.82 ± 0.26	16.59 ± 0.03	2.23	...	...	...	...	15.26 ± 0.10	13.80 ± 0.07	13.35 ± 0.08	1.46	0.45	1993 Jan 12
V410 x-ray 8d	18.51 ± 0.19	16.79 ± 0.03	1.72	...	...	...	...	14.31 ± 0.09	13.03 ± 0.07	12.47 ± 0.06	1.28	0.56	1993 Jan 12
V410 x-ray 8e[e]	19.24 ± 0.38	17.30 ± 0.05	1.94	M4:	21	1.9:	9.5::	14.63 ± 0.08	13.76 ± 0.06	12.88 ± 0.05	0.87	0.88	1993 Jan 12
V410 x-ray 8f	18.33 ± 0.17	17.06 ± 0.04	1.27	...	...	...	...	15.95 ± 0.15	14.36 ± 0.12	...	1.59	...	1993 Jan 12
V819 Tau	11.57 ± 0.01	10.45 ± 0.01	1.12	K7V	1.7	0.35	1.70	9.59	8.77	7.97	0.94	0.65	
LkCa 7	11.63	10.58	1.05	K7	4	0.28	1.40	9.26	8.56	8.33	0.70	0.23	
DE Tau	11.87	10.66	1.21	M1	54	0.19	0.95	9.15	8.26	7.71	0.89	0.55	
RY Tau	10.28	9.63	0.65	K1	21	0.23	1.15	8.00	6.78	5.74	1.22	1.04	
HDE 283592	8.34	7.83	0.51	G5	abs	0.15	0.75	7.46	7.04	6.93	0.42	0.11	
V410 anon 3	17.31 ± 0.07	15.45 ± 0.01	1.86	M4.5	2	0.09	0.45	...	...	...	...	...	
V410 anon 9	15.49 ± 0.01	13.38 ± 0.01	2.10	A2	abs	2.09	10.45	10.15 ± 0.04	8.84 ± 0.05	7.96 ± 0.04	1.31	0.88	1993 Jan 12
V410 anon 12	14.94 ± 0.01	13.29 ± 0.01	1.66	M4+	0	0.00	0.00	12.18 ± 0.04	11.63 ± 0.05	11.36 ± 0.04	0.55	0.27	1993 Jan 12
V410 anon 13	18.58 ± 0.20	15.97 ± 0.02	2.61	M5	22	0.55	2.75	12.82 ± 0.04	11.64 ± 0.05	10.90 ± 0.04	1.18	0.74	1993 Jan 12
V410 anon 17	13.81 ± 0.04	12.76 ± 0.01	1.05	M1.5	0.5	0.00	0.00	...	...	...	...	...	

NOTE.—The photometry with errors quoted is the data as described in the observations section. The data with no errorbars is drawn from the summary tables in Strom et al. 1989 except as noted.

[a] Cohen & Kuhi 1979.

[b] Kim 1990.

[c] Hartigan, Strom, & Strom 1993.

[d] Kenyon et al. 1990.

[e] These objects are the most likely counterparts to the X-ray sources among the multiple candidates examined.

5.1. *Anonymous Stars*

Because there were 97 fibers available for placement upon stars or sky positions when using the HYDRA spectrograph, we chose to place some of these fibers upon anonymous stars that fell within the area of the L1495E cloud. We obtained usable spectra for five of these stars, optical photometry for these five, and, coincidentally, near-infrared photometry for four of the stars. This data is also given in Table 3.

Other anonymous stars appeared in our infrared imaging frames. Data for these stars is also given in the Appendix.

6. STELLAR PROPERTIES

On the basis of the data tabulated in Table 3, we can assess the likelihood that we have properly identified the stellar X-ray sources and compare the distribution of the spectral types of the newly identified stars with that of the previously identified population. We must first evaluate the extinction suffered by each star. The spectral type and observed $R-I$ color give a color excess for each star, $E(R-I)$, which, when combined with a standard reddening law, yields the extinction. These values are also tabulated in Table 3.

Among the candidate objects for identification with the X-ray sources, only the spectrum for V410 X-ray 8a clearly disqualifies it as a member of the cloud population. The spectral type of V410 X-ray 8a is M0-2 III. This spectral type, combined with the available photometry, indicates substantial extinction. Since the object lies near the cloud edge, it is likely that we are viewing the star through a substantial path length of the L1495 cloud; the luminosity classification of this spectrum clearly identifies the star as a background giant. The positional discrepancy with the X-ray source location is also much too large to be acceptable. Therefore the X-ray source is most likely associated with the Hα emission object X-ray 8e, although we have no spectrum for X-ray 8d which lies marginally closer to the X-ray position. The spectrum of V410 X-ray 8e indicates that this star is heavily veiled with a spectral type near M4 or possibly later. Due to the veiling and the approximate spectral type, the reddening is poorly determined. The Hα emission is very broad. The spectra of all of the other X-ray candidate objects exhibit Hα in emission and M type spectra.

Among the anonymous stars for which we have obtained spectra, there are four M-type stars. One of these stars, V410 anon 13, clearly shows significant extinction, indicating that it cannot be a foreground star. This star has an Hα emission equivalent width of 22 Å, indicating that it is most likely a member of the cloud population of PMS stars. The other three M stars show little or no extinction ($A_v \leq 0.10$) and little, if any, Hα emission [$W(\mathrm{H}\alpha) \leq 2$ Å]; therefore they are likely to be foreground M dwarfs. The fifth star is an A2 star, showing no Hα emission, and a large extinction, 10.45 mag at V. The strength of the O I triplet at 7774 Å is consistent with the spectral type found from the Hα line profile and a luminosity class of V–III. The Hα profile indicates a main-sequence star. At a Galactic latitude of −15.5 and a Galactic longitude of 168.7, only 0.1 A III stars per square degree are expected within the volume formed by the cloud size and the distance to the star were it a giant. This star is thus most likely a main-sequence A star at or close to the cloud distance.

We can now examine the distribution of spectral types for the previously identified cloud population and compare it with that found for the newly identified population. This is shown in Figure 5. Clearly the *newly discovered cloud members include a much larger number of later type stars*, indicating that previous studies greatly undersampled the lowest mass PMS stars. We can also examine the distribution of reddening values within the two groups as shown in Figure 6. The reddening values in the previously identified population are heavily weighted toward low values with a median at 1.25 mag. The median value for the newly identified population is 3.80 mag, indicating that a major reason for the absence of these stars from previous surveys is the relatively large extinction associated with these intrinsically faint objects.

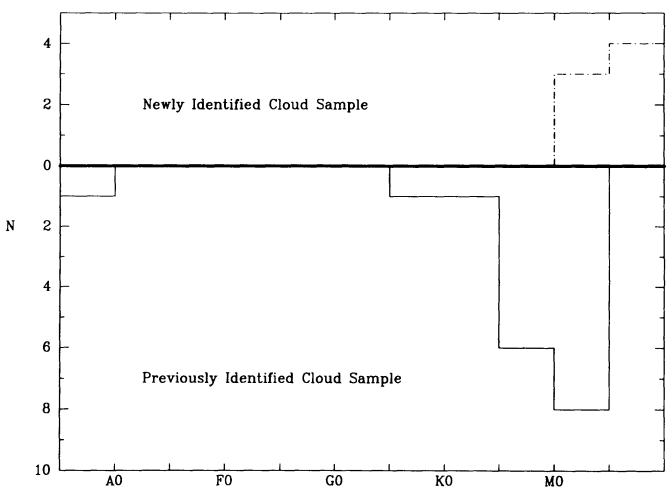

FIG. 5

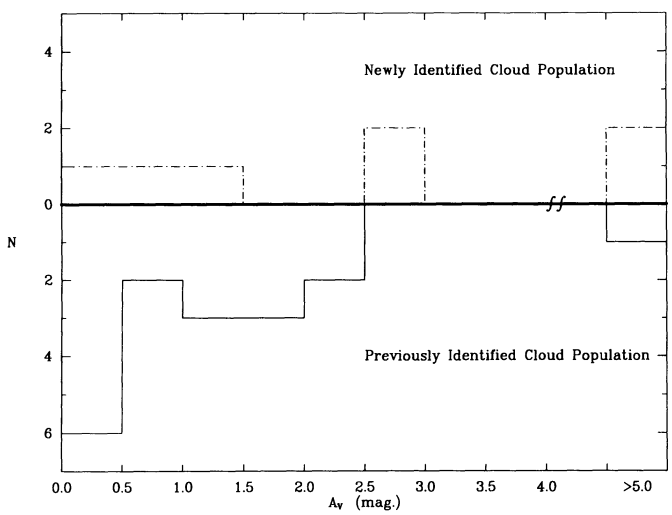

FIG. 6

FIG. 5.—The distribution of spectral types for the newly identified members of the L1495E cloud population compared with that for the previously identified cloud population.

FIG. 6.—The distribution of extinction values for the newly identified members of the L1495E cloud population compared with that for the previously identified cloud population.

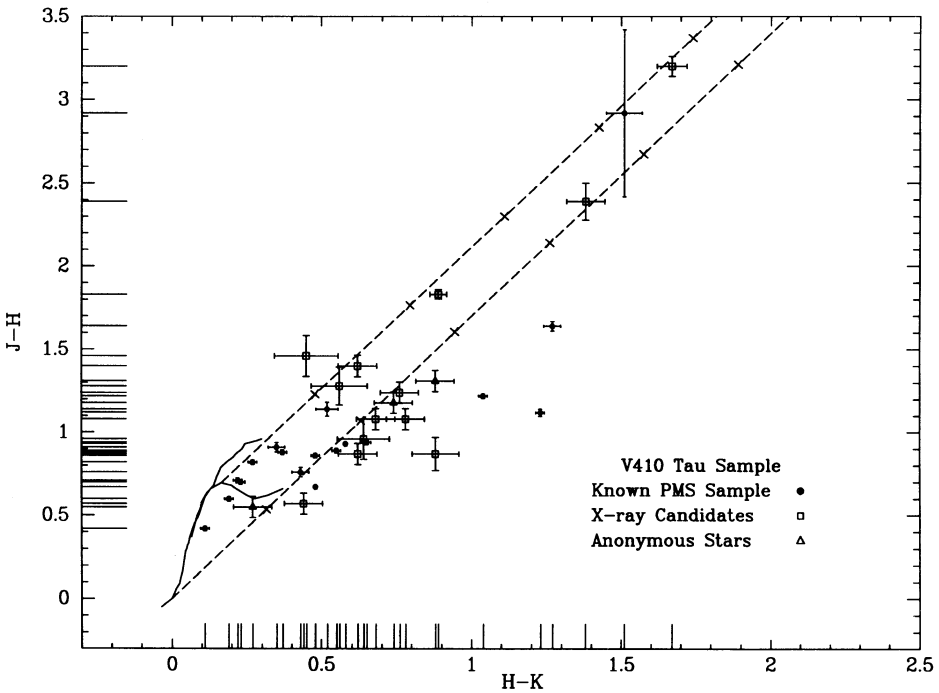

FIG. 7.—An infrared color-color diagram for the stars in the L1495E cloud. The *filled circles* show the previously identified population of L1495E. The *open squares* show the candidates for identification of the X-ray sources, and the *triangles* show the locations of the anonymous objects. The *tick marks* on the reddening lines indicate intervals of 5 mag in A_v.

6.1. *The Infrared Color-Color Diagram*

In Figure 7 we present the near-infrared color-color diagram for the stars in Table 3. The solid lines show the locus of the main sequence and of the giant branch. The dashed lines show the bounds of the region within which reddened main-sequence stars may fall. Stars lying to the right of this region show definite evidence for excess emission believed to arise from circumstellar accretion disks. Stars lying between these lines may still possess accretion disks. However, it is impossible to distinguish such stars from reddened main-sequence stars or reddened WTTS in this diagram. Also shown in the lower and left axes of this figure are the marginal distributions of all of the data for these sources. This allows us to also indicate the locations for objects too red to have measurements at all three wavelengths and allows quick evaluation of the distribution of points in each color (Tufte 1983).

We may also obtain a measure of the extinction suffered by each star from this diagram. This is useful, both as a consistency check with the optical and X-ray data, and to provide extinction estimates for objects for which we have no other extinction measure. Weak line T Tauri stars successfully deredden back to the main sequence in this diagram, using the extinction derived from the optical region photometry. However, CTTS define a different sequence when the reddening is derived from their optical colors in the red region and high signal-to-noise spectra are used to assign spectral types (Strom, Strom, & Merrill 1993). Those stars which we are able to clearly assign to one of these two classes we deredden to the appropriate sequence. We derive extinctions for the remaining stars, assuming that all of these stars are WTTSs. This procedure overestimates the extinctions for those stars which are actually CTTS owing to the fact that such stars have intrinsic excess emission arising in circumstellar accretion disks. For most stars, the extinction determined by each of these methods are in reasonable agreement. Extinctions derived in this way are used only for the four objects in Table 3 lacking optical photometry and/or spectral types. The derived values are given in Table 4.

We can see from this diagram that most of the candidates for identification with the X-ray sources are clearly PMS stars exhibiting the excess infrared emission characteristic of circumstellar accretion disks. The three apparently most heavily reddened objects are two of the X-ray discovered sources and *IRAS* PSC 04154+2823. The only candidate for identification with V410 X-ray 8 which clearly exhibits disk emission is X-ray 8e; it is the object which also has the smallest positional discrepancy and which exhibits broad Hα emission. The infrared colors of V410 anon 13 also are in agreement with assignment to cloud membership based on its observed infrared excess. The other reddened serendipitous source, V410 anon 9, is also a possible cloud member. This star has a spectral type of A2 and an inferred extinction of 10.45 mag at V. Kim (1990) detected this star in his near-infrared survey and placed it in his definite PMS group from its location in the infrared color-color diagram. While our colors are little different from his [$\Delta(J-H) = -0.16$; $\Delta(H-K) = 0.03$], we feel that this star can deredden naturally to the appropriate colors for its spectral type, given the errors in the photometry, although excess infrared emission cannot be ruled out. There is no reflection nebula associated with this star and there is no emission at Hα. Therefore it is not certain whether this star is associated with L1495E.

6.2. *The H-R Diagram*

One of the major goals of the study of a young star formation region is to place the stars in the H-R diagram to estimate the masses of the stars and their approximate ages in order to determine the rate of star formation versus time in the region. With mass estimates for the stars, we can calculate the star formation efficiency of the molecular cloud and compare the local IMF to that observed in the field. The data in Table 3 enable us to locate the population of L1495E in the H-R diagram.

TABLE 4

H-R DIAGRAM DATA FOR PRE–MAIN-SEQUENCE STARS IN L1495

ID	SpTy	A_J	J	BC_J	log T_e	$M_{bol}(J)$	L(J)	L(J_c)
FO Tau	M2	0.54	9.70	1.67	3.544	4.95	0.82	0.49
LkCa 4	K7	0.35	9.28	1.54	3.602	4.59	1.15	1.15
CY Tau	M2	0.03	9.76	1.67	3.544	5.52	0.49	0.49
LkCa 5	M2:	0.03	10.05	1.67	3.544	5.81	0.38	0.38
V410 x-ray 1	M3.5-4	0.28	10.50	1.79	3.512	6.13	0.28	0.28
V410 x-ray 3	M6	0.07	11.50	1.90	3.447	7.45	0.08	0.08
V410 Tau	K7	0.00	8.33	1.54	3.602	3.99	2.0	1.72
DD Tau	M4	0.00	9.56	1.83	3.498	5.51	0.49	0.32
CZ Tau	M3	0.50	9.90	1.75	3.525	5.27	0.61	0.42
PSC04154+2823 [a]	...	5.9	13.9	1.67	3.544	3.9	2.2	2.2
V410 x-ray 2 [a]	...	5.9	15.0	1.67	3.544	4.9	0.86	0.86
V410 x-ray 4 [a]	...	4.5	13.5	1.67	3.544	5.1	0.71	0.71
V892 Tau	B9	2.44	8.55	0.00	4.050	0.23	64.3	64.3
V410 x-ray 7	M1	2.21	11.88	1.63	3.562	5.42	0.54	0.54
Hubble 4	K7	0.69	8.56	1.54	3.602	3.53	3.1	3.1
CK Tau 1	M2:	0.58	12.50	1.67	3.544	7.71	0.065	0.065
PSC04158+2805 [a]	...	0.67	13.15	1.67	3.544	8.27	0.038	0.038
V410 x-ray 6	M5	0.23	10.54	1.88	3.477	6.31	0.24	0.24
V410 xray 5a	M5	0.79	11.88	1.88	3.477	7.09	0.12	0.12
FQ Tau	M4	0.13	10.98	1.83	3.498	6.80	0.15	0.078
BP Tau	K7	0.10	9.30	1.54	3.602	4.86	0.90	0.90
V410 xray 8e	M4:	2.7:	14.63	1.83	3.498	7.88	0.06	0.06
V819 Tau	K7 V	0.48	9.59	1.54	3.602	4.77	0.98	0.98
LkCa 7	K7	0.39	9.26	1.54	3.602	4.53	1.22	1.22
DE Tau	M1	0.26	9.15	1.63	3.562	4.64	1.11	1.11
RY Tau	K1	0.32	8.00	1.30	3.698	3.10	4.57	4.57
HDE 283592	G5	0.21	7.46	1.11	3.748	2.48	8.09	8.09
V410 anon 3 [b]	M4	0.61	15.45	0.30	3.498	9.26	0.015	0.015
V410 anon 9	A2	2.88	10.15	0.00	3.954	1.39	22.1	22.1
V410 anon 12	M4+	0.00	12.18	1.83	3.498	8.13	0.044	0.044
V410 anon 13	M5	0.76	12.82	1.88	3.477	8.06	0.048	0.048
V410 anon 17 [b]	M2	0.00	12.76	0.55	3.544	7.43	0.083	0.083

[a] Values for these stars are calculated using the extinction derived from the near-infrared colors and mean values for the bolometric correction and effective temperatures for the X-ray discovered population.

[b] Values for these stars are calculated using I as the wavelength for normalization due to the absence of near-infrared photometry.

From our knowledge of the components of the spectral energy distributions of T Tauri stars (Bertout, Basri, & Bouvier 1988; Hartigan et al. 1992), we know that the maximum contribution of the stellar photosphere to the spectral energy distribution is made at wavelengths near 1 μm. Flux variations due to rotational modulation are also small at these wavelengths (Vrba et al. 1986; Bouvier & Bertout 1989). Therefore we will choose to use the flux at I or J as our measure of the stellar photospheric flux. When data at J are available, J is preferred. We must still estimate the amount of extinction for each star, although we have minimized the importance of extinction corrections by working this far to the red. The spectral type and $R-I$ color yield a color excess for each star, $E(R-I) = 1.4\,A_J$, which, when combined with a standard reddening law, becomes an extinction at the chosen wavelength, I or J ($A_J = 0.46 \times A_I = 0.28 \times A_V$). Using the bolometric corrections of Bessell & Brett (1988), we find that the bolometric correction at I varies rapidly as a function of spectral type beyond M0, while the variation at J is slow and monotonic over the entire spectral range of interest. Therefore we will use the J magnitude, whenever possible, [corrected for extinction, distance ($m-M = 5.88$) and bolometric correction) as our measure of the stellar luminosity. Using the temperature–spectral-type calibration of Hartigan et al. (1994) compiled from the work of Bessell & Brett (1988) and Schmidt-Kaler (1982), we derive an effective temperature for each star for which we have a spectrum. The errors in placement of stars in the H-R diagram vary with spectral type. They can be estimated by using the values given below for two spectral types.

$$K5 \pm 1 \text{ subtype} \begin{cases} +0.019 \text{ in } \log T_{\rm eff} & -0.03 \text{ in } R_c - I_c \text{ and} & \text{observed}, \\ -0.020 & +0.11 \quad E(R_c - I_c) & \\ -0.02 \text{ in } A_J & -0.05 \text{ in } BC_J & \text{derived}, \\ +0.08 & +0.01 & \\ +0.01 \text{ in } \log L & & \text{result}, \\ +0.03 & & \end{cases}$$

$$M3 \pm 1 \text{ subtype} \begin{cases} +0.019 \text{ in } \log T_{\rm eff} & -0.21 \text{ in } R_c - I_c \text{ and} & \text{observed}, \\ -0.027 & +0.26 \ E(R_c - I_c) & \\ -0.15 \text{ in } A_J & -0.08 \text{ in } BC_J & \text{derived}, \\ +0.19 & +0.08 & \\ +0.03 \text{ in } \log L & & \text{result}. \\ -0.04 & & \end{cases}$$

However, the sometimes large light variations of PMS stars prove to be the largest source of random error in the placement of these stars in the H-R diagram (Hartigan et al. 1994). This can be seen immediately in Table 3 where our two observations of V410 X-ray 1 differ by more than a magnitude at J and of V410 X-ray 3 differ by more than 0.5 mag. There are multiple sources for the variability exhibited by PMS stars. Rotational periods have been determined for many PMS stars by observation of the spot modulation of their light curves. The amplitude of this variation may be as small as a few hundredths of a magnitude or as large as 1 mag (at V) (AA Tau; Vrba et al. 1988). These stars are also known to have an irregular component to their variability with very large amplitudes sometimes exceeding several magnitudes (Herbig & Bell 1988). These irregular fluctuations are presumed to be due to variations in the accretion rate through the disks of these stars (Kenyon et al. 1994). In the extreme case, an FU Ori event may cause a rise of more than 5 mag over a relatively short period of time (weeks) with a much longer decay time (years) (Hartmann, Kenyon, & Hartigan 1993). Hartigan et al. (1994) found that the error in placement of PMS stars in the H-R diagram was dominated by the variability of these stars. They estimated that variability was responsible for $\sigma \simeq 0.05$ in $\log L$ although there is a long tail at higher amplitudes to the distribution. When all of the possible sources of error are combined in quadrature, the result is a "typical" 1 σ uncertainty of 0.08 in $\log L$.

The data placing each of our stars in the H-R diagram is given in Table 4 and they are plotted in Figure 5 with the 10^8 yr isochrone from the D'Antona & Mazzitelli (1994) evolution tracks. The objects V410 X-ray 2, 4, PSC 04154+2823 and PSC 04158+2805 are placed in the H-R diagram using the (uncertain) extinctions estimated from their near infrared colors, a bolometric correction and effective temperature assuming they are middle M stars similar to the other objects found in this sample. For V410 anon 3 and 17, for which there was no near-infrared photometry, we used I as the standard wavelength. The final luminosities for the five objects known to be binaries are then corrected for the light contributed by any secondary star discovered by high spatial resolution observations (see § 5.3). These final values are given in column $L(J_c)$.

It is obvious from Figure 8 that the stellar population of L1495E is very young. However, it is difficult to evaluate exactly how young and how coeval this population is because different sets of "modern" evolutionary tracks (D'Antona & Mazzitelli 1994; Swenson et al. 1994) show sufficient differences to make interpretation difficult. Also, the isochrones are in intervals of log age; therefore the stars are evolving very rapidly in the upper part of the H-R diagram and more slowly as they age. In Figure 9 we show the data for these stars plotted on (1) the D'Antona & Mazzitelli tracks using the Alexander opacities and the Canuto and Mazzitelli

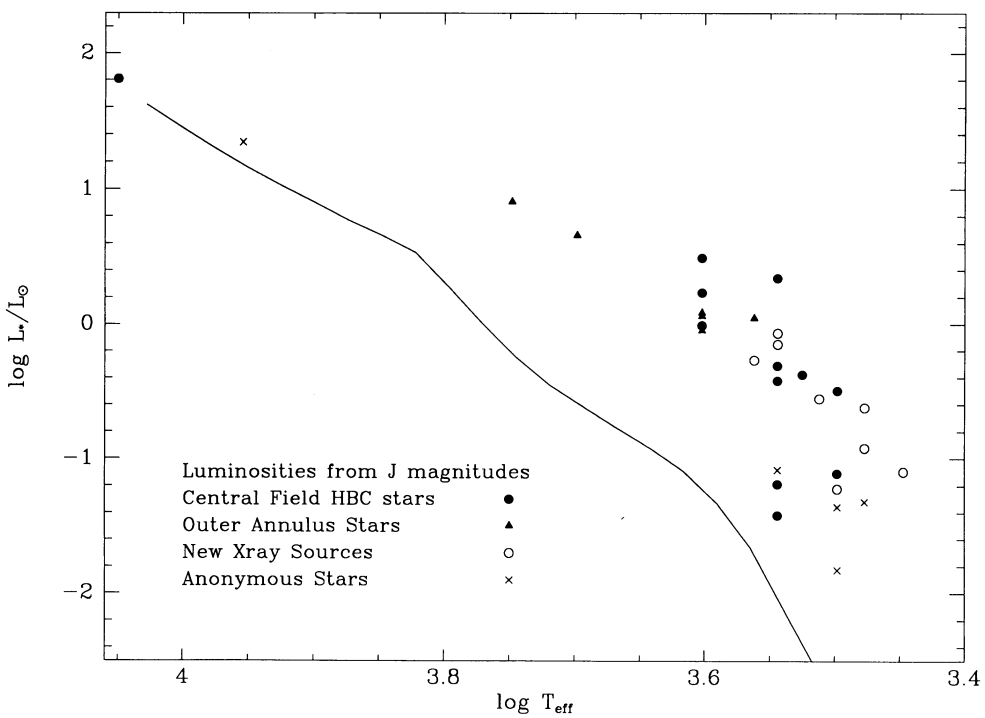

FIG. 8.—An H-R diagram for the stars in the L1495E cloud showing only the locations of the objects and the 10^8 yr isochrone of D'Antona & Mazzitelli (1994)

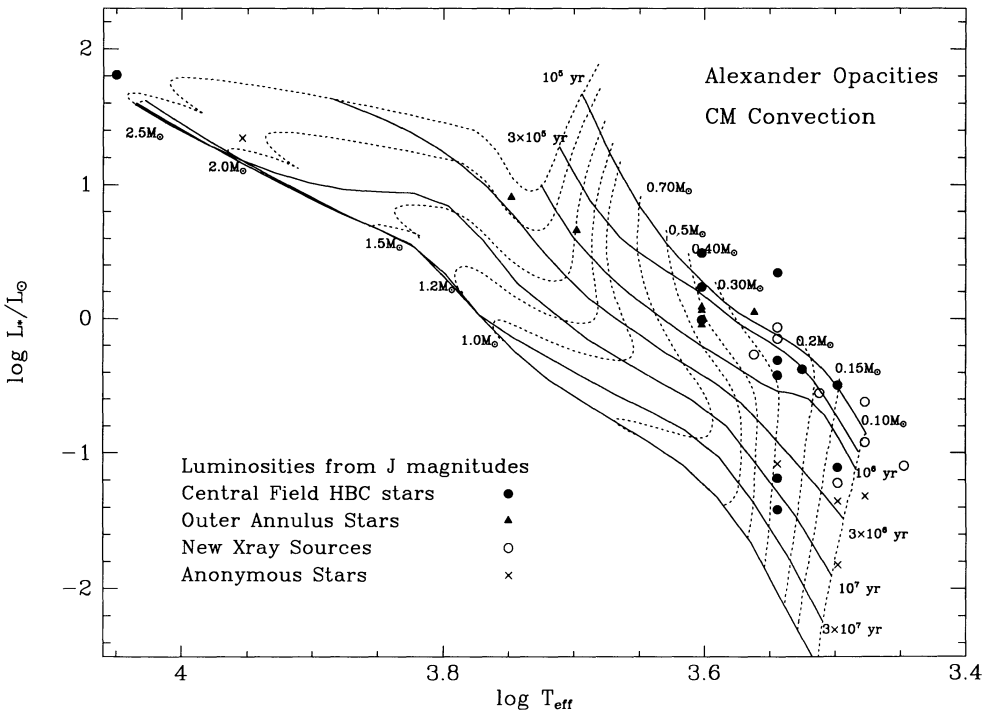

FIG. 9*a*

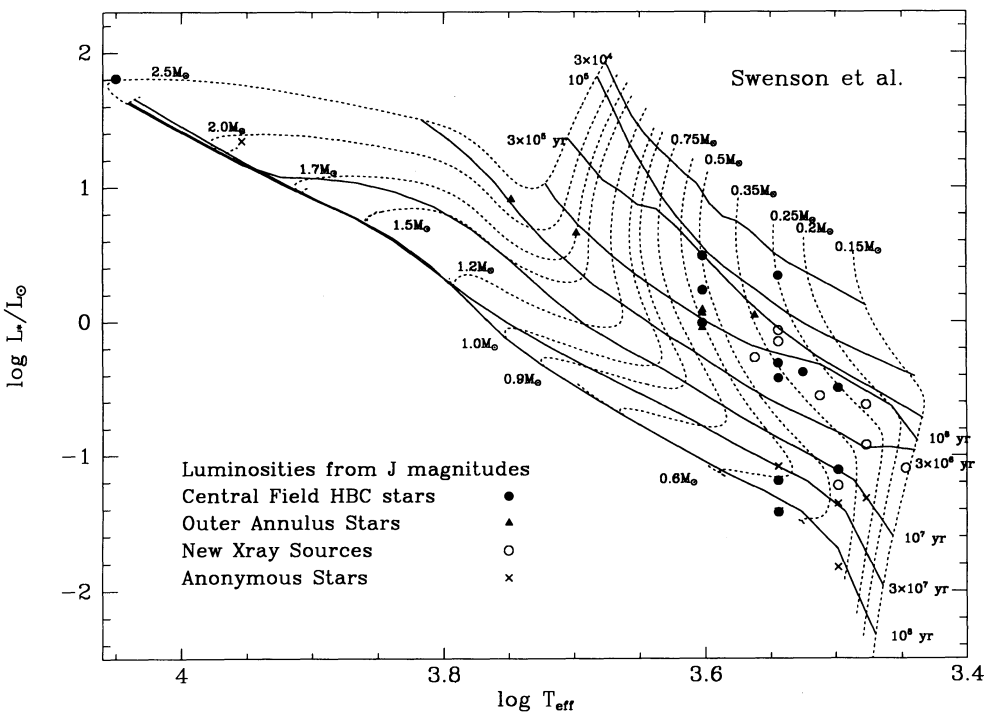

FIG. 9*b*

FIG. 9.—Comparison of the stellar luminosities and effective temperatures for the stars in L1495E with two sets of recent PMS evolutionary tracks. (*a*) The PMS tracks of D'Antona & Mazzitelli (1994) using the Alexander opacities and the convection formulation of Canuto & Mazzitelli, and (*b*) the PMS tracks of Swenson et al. (1994).

convection formulation; and (2) the Swenson et al. tracks. It is clear that, for stars this young ($\leq 10^6$ yr) the tracks differ sufficiently to influence our estimate of coevality as well as the "absolute" age. On the D'Antona & Mazzitelli tracks, for stars with masses less than 0.5 $M_\odot$, the population appears approximately coeval with an age of $t \sim 5 \times 10^5$ yr. Using a program written by P. Hartigan which interpolates between the isochrones to assign an age to each star, we find that 20 of the 22 low-mass PMS stars, excluding those viewed by scattered light (see later in this section, and the anonymous stars, have ages $\leq 7.1 \times 10^5$ yr. On the Swenson et al. tracks, for the same mass range, the apparent age increases as the mass decreases and the mean age for the L1495E population is 10^6 yr. Given the uncertainties in the model isochrones and the fact that the models are still sensitive to initial conditions at these early ages, this group can be considered coeval to within ≤ 1 Myr. The two apparently older stars merit discussion. We have only one complete set of colors for FQ Tau. However, at the time of the Leinert et al. (1992) speckle observations, FQ Tau was more than 0.5 mag brighter at K than when we observed the star. If this brightness change is also reflected at J, this star is then $< 1\ \sigma$ above the mean age for the group. The remaining star lies 3.75 σ above the mean age of the group; this is not unreasonable for a sample this size.

One possible problem apparent from both sets of tracks is the gradually increasing age found for stars with masses $\geq 1.5\ M_\odot$. While RY Tau and HDE 283572 lie off the face of the cloud, V892 Tau (Elias 1) is heavily embedded in the cloud core and illuminates a reflection nebula. It is difficult to believe, given the apparent velocity dispersion of L1495E of ~ 3.0 km s^{-1}, or 3.0×10^{-6} pc/yr^{-1}, that this star is over 3×10^6 yr old as the tracks imply. A star formed in the center of the cloud would have moved more than 200′ away from the cloud center in 3×10^6 yr. The motion of this star would have to be aligned within 10° of the line of sight and be moving away from us in order to remain located in cloud center and still exhibit an extinction of 9 mag. The only alternative (other than suspecting a systematic error in the tracks) is that the age of this star is correct and that star formation actually began 3×10^6 yr ago. In this case the timescale for "building" a star via infall and accretion, before it appears on these tracks, would have to be much longer for low-mass stars.

From examination of Figures 8 and 9 and Table 4, several objects deserve special mention. There are two members of the previously identified PMS population that fall well below the main body of the distribution. The images of these objects, CK Tau 1 and PSC 04158+2805, appear definitely extended on our deep R and I frames, the PSC object appearing triangular and the object near Hubble 4 appearing flamelike (Fig. 10). We suspect that we are not seeing these objects directly but instead via light scattered through a circumstellar envelope or from nearby molecular cloud material. Recent submillimeter observations of low-luminosity embedded sources in the Taurus region (Barsony & Kenyon 1992) indicate very large extinctions for these sources, ($50 < A_V < 600$),

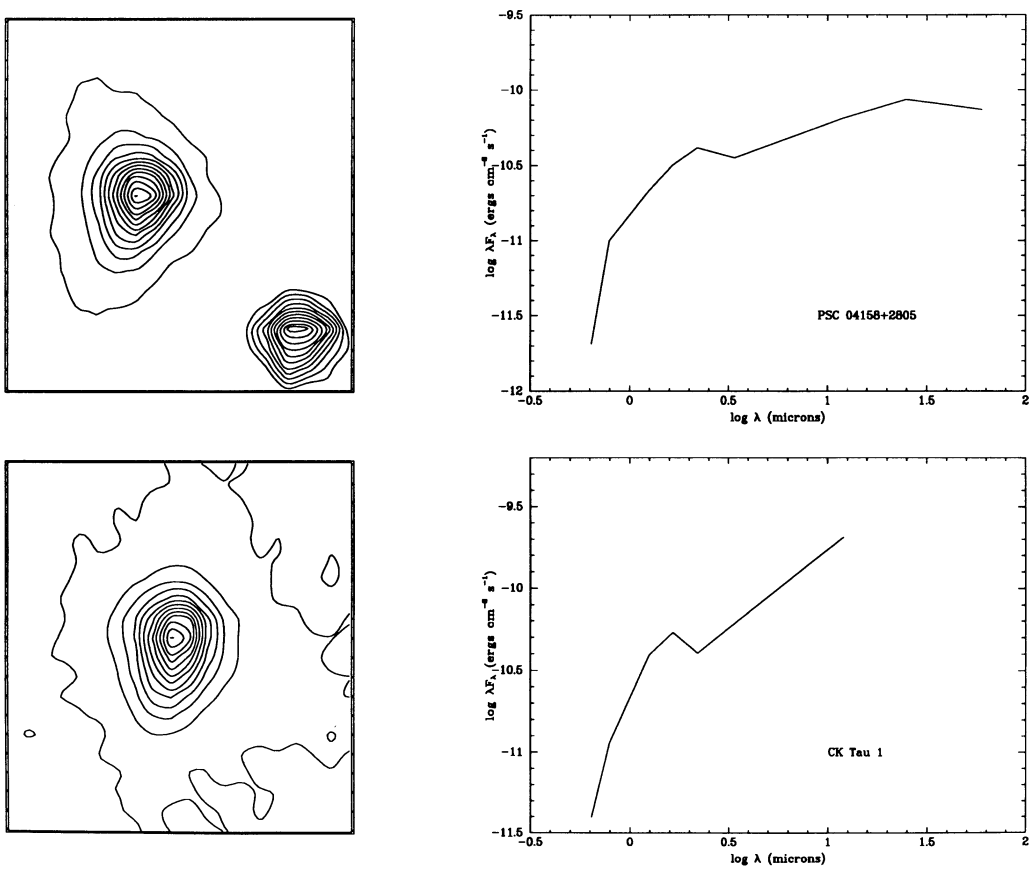

FIG. 10.—*Left:* contour plots of the I-band images of CK Tau 1 and PSC 04158+2805. The plots are 20 pixels on a side and the plate scale is 0.″78 pixel^{-1}. In the lower right-hand corner of the first contour plot is shown the point spread function as exhibited by a nearby star of similar brightness. *Right:* plots of the spectral energy distributions of the two sources. Both objects show the secondary bump in the spectral energy distributions characteristic of objects seen via scattered light.

sufficient to render them undetectable even at 2 μm. However, these objects are nevertheless visible in the near infrared and sometimes at even shorter wavelengths. This paradox can be resolved if the density distribution surrounding these objects is highly asymmetric. Models of sources such as these using asymmetric density distributions have been developed recently by Kenyon, Calvert, & Hartmann (1993a) and Kenyon et al. (1993b). These authors find it necessary to introduce a bipolar hole in the density distribution in order to reproduce both the observed spectral energy distributions and the extended images of such sources. Both the spectral energy distributions and direct images of the objects shown in Figure 10 are very similar to those represented by these models. the $(R-I)$ colors of these objects indicate 5–10 mag of extinction. However, the models of Kenyon et al. (1993b), while only calculated for the J, H, and K bands, suggest that the actual extinction that should be applied to the observed magnitudes could be a factor of 3 or more higher than that inferred from the observed near-infrared colors. The discrepancy should be even greater for extinctions determined from the $R-I$ color. the visible and near-infrared light is due to scattering and not transmission, and therefore the anomalous location of these stars in the H-R diagram can easily be accounted for by an underestimate of the extinction.

Our spectral type for CK Tau 1 is uncertain as the spectrum appears heavily veiled and contains strong emission lines of H, [O I], [S II], [Fe II] among others. This contributes a major source of error in the reddening estimate as we are probably not measuring photospheric colors. Our previously published images of CK Tau 1 in Hα (Strom et al. 1986) indicated a faint bipolar jet emanating from this star. The recent narrow-band imaging by Goodrich (1993) confirms this result, showing a bipolar jet clearly in the [S II] images.

Among the X-ray discovered sources in this cloud, it is clear that V410 X-ray 1, 2, 3, 4, 5a, 6, 7, and 8e are member of the PMS population of L1495E. In most cases they are the only possible optical object which could be identified with the X-ray source. The near-infrared colors of these objects indicate excess infrared emission. When we have spectra for these objects, Hα appears in emission [W(Hα) $\geq$ 8 Å]. As discussed previously, X-ray 8a is a background M giant seen through the edge of the cloud. We can make no statement about the possible association of V410 X-ray 8b, 8c, 8d, 8f, and 5b since we have no spectra for those objects.

Of the serendipitously observed stars, V410 anon 3, 12, and 17 show little or no extinction or Hα emission. Their derived luminosities (at the distance of the Taurus clouds) place them above the main sequence. However, they are more likely *main*-sequence stars in front of the cloud. The Galactic model (Bahcall & Soneria 1980) predicts $\sim$10 M stars between us and the Taurus clouds projected on the central region of the cloud ($r \leq 25'$). The other two serendipitously observed stars may well be members of the cloud population. V410 anon 13 has an Hα emission equivalent width of 22 Å and an inferred extinction of 2.75 mag at V. This star is clearly a strong candidate for inclusion in this young group. The lack of detection in the *ROSAT* image is probably due to its low luminosity, below that of any of the X-ray–detected objects. The star V410 anon 9, discussed previously appears to be a normal A2 star with no Hα emission. When dereddened and placed at the distance of the Taurus clouds, the star lies just above the main sequence, not far below V892 Tau. It is possible that this star lies behind the cloud, but it cannot lie far behind because the probability of finding an A giant this far above the Galactic plane is small.

6.3. *Binaries in L1495E*

While we have approximately doubled the previously known population within the central region of L1495E, all with M stars, it is still possible that even more low-mass stars may be hidden as secondaries in binary systems. Fortunately there has been much recent high spatial resolution work which allows us to evaluate this possibility (Ghez 1993; Simon et al. 1992; Leinert et al. 1992; Simon 1992; Ghez, Neugebauer, & Matthews 1992).

Of the previously identified PMS sample (19 stars), seven are known to be binaries (V410 Tau, DD Tau, CZ Tau, V892 Tau, FO Tau, FQ Tau, and LkCa 7). Eight stars were found to be single at the separations, flux ratios (and sometimes position angles) to which the measurements were sensitive. Four stars (CK Tau 1, PSC 04154+2823, PSC 04158+2805, and LKCa 5) were not examined. V892 Tau was discovered to be a binary by Thornley et al. (1989) using near-infrared imaging. The secondary was later confirmed by Skinner, Brown, & Stewart, (1993) in their VLA observations of this region. They detected both V892 Tau and its close companion to the NE as well as CK Tau 1 and Hubble 4 (Skinner 1993).

While a few B and A stars in young stellar groups have been identified as possible X-ray sources (Caillault & Zoonematkermani 1989; Strom et al. 1990; Pravdo & Angelini 1993), there is always the possibility that the X-ray emission is attributable to a low-mass companion (Schmitt et al. 1985). In this case, it is reasonable to attribute the X-ray luminosity of V892 Tau to the low-mass secondary of the system. The derived X-ray luminosity is consistent with the inferred luminosity of the secondary if we assume that the luminosity ratio of the two components of V892 Tau is close to the ratio of their infrared luminosities, the star lies on the mean isochrone for this group, and we use the bolometric correction inferred from this placement.

Flux ratios are in general available at only one wavelength for these binaries, usually K (2.2 μm). For five of the seven known binaries, the flux ratios at K lie between 1.1 and 2.2. The other two stars (V892 Tau and V410 Tau) have relatively much fainter companions. If we assume that this ratio represents the true luminosity ratio of the components, the extinction for both components is the same, and that they lie on the 10^6 yr isochrone, we can estimate the masses of these stars. Therefore these seven companions can also be added to the low mass ($M < 0.3\ M_\odot$) population of the cloud.

6.4. *The Cloud IMF*

Among the basic problems to be addressed by studies of star formation are (1) to derive the initial mass function (IMF) for isolated star formation regions and compare with that derived from study of stars in the solar neighborhood; and (2) the local efficiency of star formation in the star-forming cores. Implicit in the determination of the IMF is the question of whether stars of mass lower than that in which hydrogen burning can be sustained (brown dwarfs) are plentiful and may therefore contribute to solving the "missing mass" problem.

It is now possible to estimate the star formation efficiency of the L1495E cloud. The mass of the cloud has been estimated at

between 180 and 230 $M_\odot$ (Ohnishi & Mizuno 1993). The total stellar mass in the central region of the cloud depends slightly on the set of tracks used to make the mass estimate. If the Swenson et al (1994) tracks are used, the total stellar mass is estimated at $\sim 13 M_\odot$; if the D'Antona & Mazzitelli (1994) tracks are used, the total stellar mass is estimated at $\sim 10.5\ M_\odot$. This leads to star formation efficiencies between 5% and 7%. If the stars in the outer region of the cloud are included, the star formation efficiencies increase to between 8% and 9.3%. Current constraints on the formation of bound clusters (Lada, Margulis, & Dearborn 1984) require that at least 30% of the cloud mass must be converted to stars. Unless a large number of low-mass members of the this group remain hidden within the cloud, at luminosities below the limit reached by this *ROSAT* exposure, it is unlikely that this group will remain bound.

One of the first studies to examine the distribution of spectral types in nearby star-forming regions was carried out by Cohen & Kuhi (1979). While a small number of stars later than spectral type M0 were found in Taurus, those authors assumed that the flattening of the mass spectrum at low masses apparent in their data, was a selection effect due to a magnitude cutoff. Since that work, there have been several surveys aimed at increasing the known PMS population of the Taurus clouds: the proper motion surveys of Jones & Herbig (1979), Hartmann et al. (1991), and Gomez et al. (1992); the Ca II H,K emission survey of Herbig et al. (1986); the X-ray sources from *Einstein* pointed observations (Walter et al. 1988); and the deep Hα emission survey of Briceño et al. (1993). The recent proper motion surveys, (Hartmann et al. 1991; Gomez et al. 1992) have found a small number (seven) of additional members of the Taurus PMS population, usually late-type stars (SpT later than M3) with relatively weak Hα emission. Most recently, Briceño et al. (1993) have used very deep ($V \approx 18$) objective prism Hα emission surveys to search for as yet undetected pre–main-sequence stars in the Taurus clouds. They identified 12 new T Tauri stars, (5) of which were found in L1544, a region previously unsurveyed in Hα and containing only one identified PMS star. Most of the newly discovered PMS stars are classical or strong emission T Tauri stars (CTTS). The PMS evolutionary tracks used until this point (Cohen & Kuhi 1979; Strom et al. 1989b) have identified the peak of the N(SpT) distribution in the Taurus clouds (K7-M0) with stars of $\sim 1\ M_\odot$ with the number of stars decreasing with mass until few stars are found below $0.4\ M_\odot$. This result is in marked disagreement with the IMF derived for the solar neighborhood. The IMF found for the local solar neighborhood (Scalo 1986; Kroupa, Tout, & Gilmore 1990, Tinney, Mould, & Reid 1992) can be well fitted by a log normal function peaking at $\log M = -0.5$ and then either decreasing as the mass decreases or possibly staying constant for all lower masses. The PMS stars identified in the above surveys have spectral types with either M or continuum + emission characteristics. Their *R* magnitudes range from 14.2 to 18.5. Even though most of these newly discovered stars are M stars, the apparent deficiency of low-mass stars remained.

One possibility for hiding additional low-mass stars is as secondaries in binary and multiple systems. Recent studies (Ghez 1993; Simon et al. 1992, Leinert et al. 1992 have suggested that most stars form in multiple systems. this possibility must also be evaluated in order to fully account for the IMF in star-forming regions.

It is also important to note that the masses for these stars obtained from the "modern" tracks are quite different from those obtained in the past. Here stars that were recently considered as typical $1\ M_\odot$ PMS stars are now found to be $0.3–0.5\ M_\odot$ stars. While this may seem a small change, these typical TTS will not be G stars when they arrive on the main sequence but early M stars. This change may have a significant effect on the analyses of disk stability and binary period distributions (Ghez 1993; Leinert et al. 1992) since derived ratios of disk mass to stellar mass will increase and the total system masses for binaries will decrease.

As a consequence of (1) the newly discovered low mass members of the L1495E cloud population (X-ray detections, eight stars; anonymous stars, one star; low-mass companions, seven known), and (2) masses derived from new tracks, the apparent deficit in the population of the low-mass end of the IMF in this part of the Taurus clouds will be decreased considerably (see below).

The combination of newly observed and already known PMS stars in L1495E enables a modern discussion of the IMF. Since we have a deep survey only in the central region of the *ROSAT* field, we will use only the objects (known and newly discovered) that fall within that area. We begin with the 12 previously known members of the cloud population. To this we add eight X-ray discovered PMS stars, one certain PMS star from the group of anonymous optically visible stars projected upon the cloud, one possible addition to the intermediate mass star population associated with the cloud, and, finally, the five known secondary stars to the cloud members within the central region that have been observed at high spatial resolution. This gives a total of 27 probable cloud members within a circle of radius 25′, centered on V410 Tau.

In order to construct an IMF for the PMS population of this cloud, we must infer a mass for each star from its position in the H-R diagram relative to the calculated evolution tracks. Here we must deal with the problem that the mass deduced for each star differs depending on the tracks we choose to use. This is particularly true at the very low mass end of the range in which we are interested, where the two sets of tracks are most divergent. We construct an IMF for each set of tracks in order to better compare the derived shape of the cloud IMF. The results are presented in Fig. 11. The results from both sets of tracks yield IMFs that peak at $\log M = -0.5$, identical to the result found by Scalo (1986) from solar neighborhood stars. There are too few stars of masses greater than $\sim 1\ M_\odot$ to allow us to draw any conclusions about the higher mass end of the IMF in L1495E, and the behavior of the derived IMF for masses below the peak is dependent upon the tracks chosen. While the IMF drops toward lower masses, the drop is much more severe for the Swenson et al. tracks. If the D'Antona & Mazzitelli tracks are used, 10 stars are found in the 2 bins of lowest mass ($-1.2 \leq \log M \leq -0.8$), while if the Swenson et al. tracks are chosen, only two stars are found in these bins. For this reason, and because (1) less than half of the cloud members have been searched for companions of subarcsecond separation; and (2) there is no knowledge of binary systems with separation below the sensitivity of current instrumentation, we are unable to make a definitive statement about the shape of the cloud IMF at these low masses. However, there is *no evidence for a rise toward lower masses* if the PMS population we have identified is either complete or representative.

We have attempted to estimate the number of possible additional members of the cloud population from our near-infrared images. In addition to deriving the *JHK* magnitudes for the candidate X-ray sources, we also obtained near-infrared magnitudes for all other objects appearing within these frames. Most of these objects, in the frames away from the cloud edge, are quite faint. Consequently, the photometric errors are larger and their colors are less definitive than we would like for the purpose of identifying

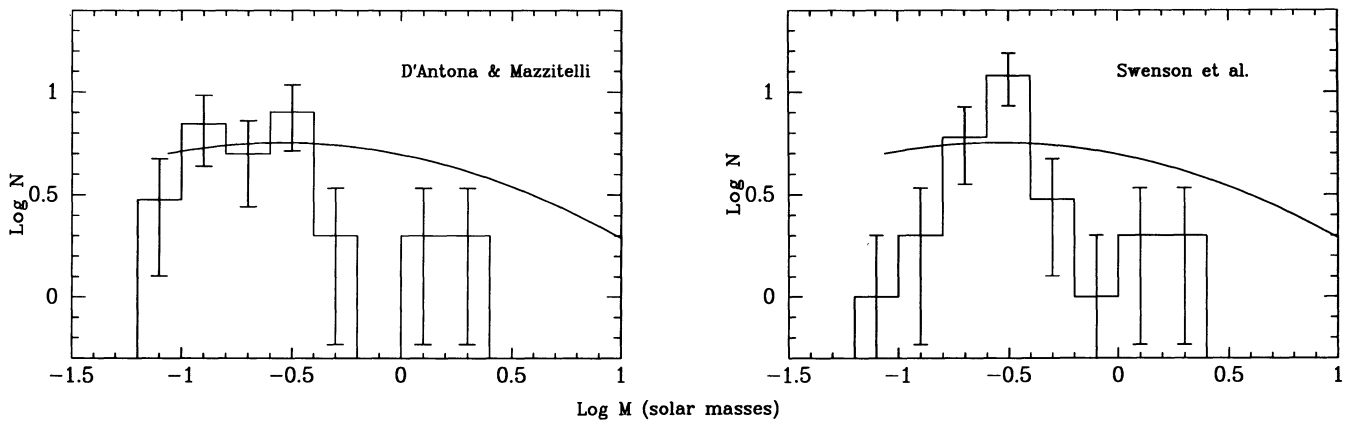

FIG. 11.—Histograms depicting the implied IMF for the cloud PMS population. The first histogram shows the IMF derived if one uses the D'Antona & Mazzitelli PMS tracks to infer stellar masses. The second histogram shows the IMF derived if the Swenson et al. tracks are used. The curve shown represents the Scalo field IMF. The error bars shown represent only $\sqrt{N}$ errors.

possible cloud members. However, there are clearly some stars (eight) whose presence in the central area of the cloud and whose colors (indicating the presence of disk emission) suggest that they are members of the cloud population. One of these stars, not visible on our long I image, just 40″ south-southeast of V410 Tau, is brighter than $K = 10$ and extremely red. Some of the stars in the region near V892 Tau are so red that no J magnitudes can be obtained; however, they cluster about the tight group of stars found in this region, suggesting membership. Table 6 gives the approximate coordinates of these stars and their photometry in the Appendix.

We must emphasize again the need for very deep X-ray searches of star formation regions in order to locate the low-mass members of the PMS population. The lack of other comparably deep observations of star-forming regions with *ROSAT* while the PSPC was operative is extremely unfortunate.

Other nearby star formation regions have not shown a deficiency of M stars comparable to that seen in Taurus-Auriga. Hughes & Hartigan (1992) compare the spectral type distribution in the Chamaeleon II cloud with that seen in Taurus. They find a higher fraction of stars with late spectral types in Cha II than are seen in Taurus. Krautter & Kelemen (1987) show the distribution of spectral types for the Lupus star formation region, at a comparable distance, which has only two stars earlier than K5 while 47 stars later than M0 are found. The new PMS evolution tracks can explain the difference in the spectral-type distribution between the Taurus and the Lupus clouds. The mean age of the stars in the Lupus clouds is considerably older than that of the stars in the Taurus clouds (Hughes & Hartigan, private communication). Therefore, using the "modern" tracks, as shown in Figure 9, the mean spectral type of the population will be considerably later in Lupus than in Taurus for the same distribution of stellar masses since these tracks take a considerable turn to lower effective temperature after $\sim 1 \times 10^6$ yr.

7. CORRELATIONS OF X-RAY PROPERTIES WITH THE STELLAR PARAMETERS

Because the X-ray emission from PMS stars appears to be consistent with coronal emission models, the strength of the X-ray emission should be correlated with the strength of the dynamo generating the stellar magnetic field. In turn, we expect that a measure of the rotation of the star will be the proper surrogate for the dynamo strength; and therefore that stellar rotation should correlate with the X-ray emission. However, one complication in this chain of logic is the fact that these very young stars are completely convective, and the currently favored dynamo models operate at the interface between the convective and the radiative zone, driven by differential rotation. However, there is a distributed dynamo model (Rosner 1980) that works thoughout the convection zone.

In this section we will evaluate the simplest correlations that we can make, the correlation of the X-ray luminosity with the stellar luminosity and with the rotational velocity. In these correlations, we will omit the data for V892 Tau since it is likely that the X-ray emission is due to the fainter component of the system for which we are unable to establish a reliable luminosity estimate since we have no spectral type.

Our X-ray data consist solely of measured values with no upper limits, therefore we have no need to use survival statistics methods in our analysis. The X-ray luminosity and the stellar luminosity are strongly correlated, with a formal probability of <0.001 that they are uncorrelated. The slope of the relationship between $\log L_x$ and $\log L_*$ found from a least-squares solution is 1.80 ± 0.01. However, since the values of $\log L_x$ are instantaneous snapshots of highly variable sources, the accuracy of the slope determination is no doubt worse than that quoted. This relationship is shown in Figure 12. The WTTS, CTTS and stars that are no longer fully convective are indicated. While there is considerable overlap between the CTTS and WTTS, the WTTS are clearly systematically more luminous than the CTTS. While it is true that some of the WTTS are found at earlier spectral types than are the CTTS and therefore at higher stellar luminosities, it also appears to be true that the WTTS are more luminous at X-ray wavelengths than the CTTS when compared at constant stellar luminosity. DD Tau is plotted twice in this figure, at its preflare and flare locations. The preflare location falls just below the center of the band, in the midst of a group of other points, while the flare point lies well above the majority of the points. It is possible that the other points lying well above the major part of the distribution represent stars that were not in their quiescent state at the time of the observation. It is also interesting to note that the X-ray luminosities of the least luminous of these PMS stars are comparable to those of the young near main-sequence K and M stars of

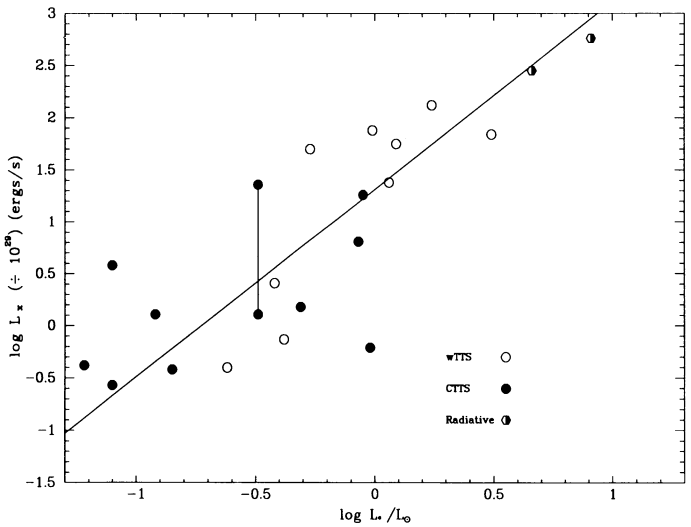

FIG. 12

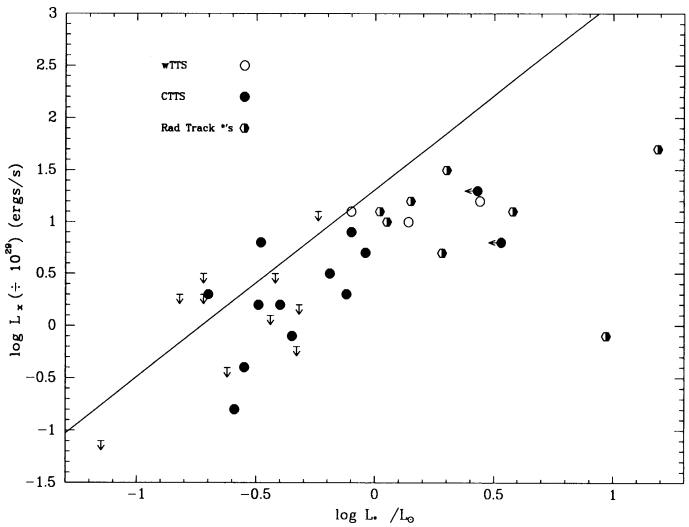

FIG. 13

FIG. 12.—A plot of the X-ray luminosity of the L1495E PMS stars vs. their stellar luminosities. The line shows the best fit to this data. The symbols distinguish the WTTS, the CTTS and the two stars that have evolved off their fully convective tracks and have developed radiative cores.

FIG. 13.—A plot of the X-ray luminosity of the Chamaeleon I PMS stars vs. their stellar luminosities. The line shows the best fit to the L1495E data. The symbols are the same as in Fig. 12.

the Pleiades (Stauffer et al. 1993). In fact, because our detection limit is lower than that of the Pleiades observations, some are even less luminous than the upper limits found for the undetected Pleiades members. This must be taken into consideration when testing dynamo models and angular momentum evolution scenarios.

We can compare this distribution with that found for the PMS members of the Cha I cloud (Feigelson et al. 1993). These authors find a correlation with with a slope of 1.00 ± 0.15 for the relationship between the stellar luminosity and the X-ray luminosity for the Cha I stars. For the stellar luminosities they used the values found by Gauvin & Strom (1992) adjusted for the closer distance that they chose to use. Since in this relationship the distance enters in the same manner on both axes, it does not matter which distance is chosen. However, the method by which the stellar luminosity is calculated has now been improved. In order to remove any systematic effects introduced in this way, we have recalculated the stellar luminosities for the Cha I stars using the J magnitude as our measure of the stellar photosphere as discussed in § 6.2 and using the same data compiled in Gauvin & Strom (1992). The X-ray luminosities are taken from Feigelson et al. (1993). In Figure 13 we have plotted the data for Cha I with the relationship derived for the stars in L1495E and shown in Figure 12. We can clearly see that the Cha I CTTS, fainter WTTS, and radiative track stars exhibit the same slope to this relationship as found for the stars in L1495E; however, they have systematically lower X-ray luminosities at constant stellar luminosity. The stars deviating from this relationship are the most luminous stars in the cloud (excluding the two A stars not considered here). Most of these stars are no longer fully convective; the most luminous WTTS lies on the boundary of the fully convective region. The only real anomalies are the two CTTS (VW Cha and WW Cha). One of these, VW Cha, is a binary with a separation of 17″ (Reipurth & Zinnecker 1993; Schwartz 1977), both components of which must lie within the X-ray beam. Reexamination of the spectra of these stars (Appenzeller, Jankovics, & Krautter 1983) shows that these stars would better be classified as continuum + emission stars leading us to overestimate the stellar luminosity for two reasons: (1) the flux at J is contaminated by disk emission and (2) the assigned early K spectral types are most likely too early leading us to use a bolometric correction too small.

There is no simple way to make a correction to the luminosities assigned to these stars, short of obtaining high-resolution spectra. Therefore we merely indicate that the stellar luminosities for these stars are upper limits. The relative absence of WTTS in this region is no doubt due to the fact that the stars with adequate photometric and spectroscopic data are those which were discovered by Hα emission surveys. Many more cloud members have been discovered in the X-ray emission surveys and in more sensitive Hα emission surveys (Hartigan 1993), but as yet lack the information necessary to place them in the H-R diagram.

An interesting aspect of this diagram is that the X-ray luminosity of stars which are now on their radiative tracks appears to be decreasing faster with the age of the star than do the X-ray luminosities of stars still fully convective. This could reflect the fact that the surface magnetic field strength is relatively weaker for these stars and therefore that the dynamo generation mechanism is not as efficient as that in the fully convective stars. A possible correlated effect has been seen by Edwards et al. (1993) in the angular momentum statistics of these stars. While the circumstellar disk appears able to regulate the rotation period of the fully convective stars quite efficiently through the linking of the stellar magnetic field with the disk, this process appears to be less efficient in stars that have radiative cores.

Another way to look at the correlation of rotation with coronal heating is to use the relationship first proposed by Bouvier (1990) between X-ray surface flux and rotational period of the star. We are fortunate to have six rotational periods determined for the stars in L1495E (Rydgren et al. 1984; Bouvier et al. 1986, 1993; Vrba et al. 1986; Walter et al. 1987; Vrba et al. 1988), and also $v \sin i$ data (Hartmann et al. 1986; Hartmann & Stauffer 1989) for this group. There are many fewer rotational periods determined in Cha I (Bouvier & Bertout 1988). In order to make use of a larger database, we will translate the rotation periods into projected equatorial

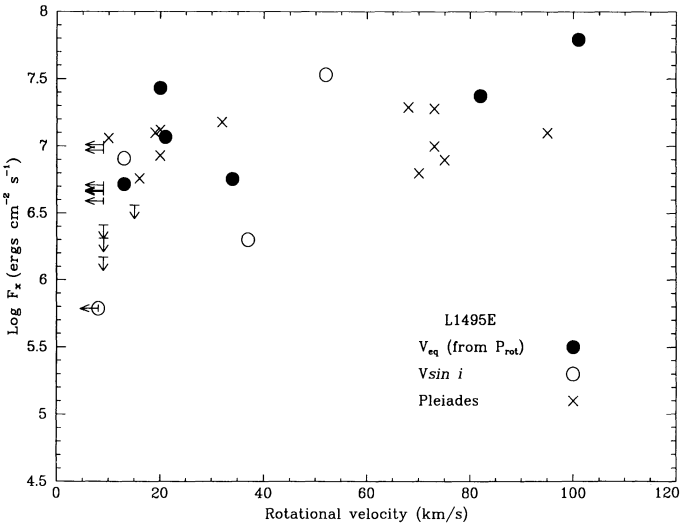

FIG. 14*a*

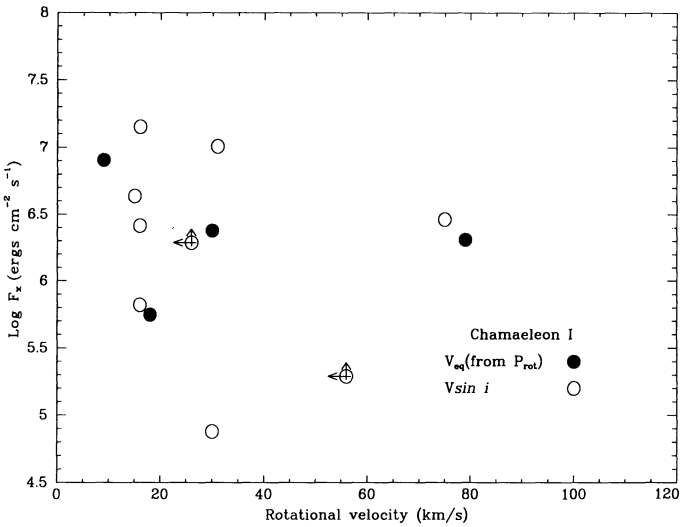

FIG. 14*b*

FIG. 14.—(*a*) A plot of the X-ray surface flux vs. the equatorial rotation velocity for the stars in L1495E and for the Pleiades (Stauffer et al. 1993). The filled points represent V_{eq} values derived from observed rotation periods. The open points represent V sin i values. The crosses show the Pleiades V sin I data. (*b*) The corresponding data for the Cha I stars. The meaning of the symbols is the same as in the previous figure. The two points with arrows superposed, show the direction of corrections expected in the rotation velocity and X-ray surface flux due to the heavy veiling of these two stars. See discussion in § 7.

velocities through knowledge of the stellar radius. In Figure 14*a* we show the relationship between log F_x and rotational velocity. Those velocities that are derived from rotation periods are shown by filled circles, while those known only from measurement of stellar line widths are marked with open circles. In Figure 14*b* the same relationship is shown for the Cha I cloud stars; the v sin i values are taken from Franchini et al. (1988) and Walter (1992). The two stars marked with limiting values in both rotational velocity and surface flux are VS Cha and WW Cha, mentioned earlier. These stars are very heavily veiled, and therefore the luminosity and thus the radii are probably over estimated, leading to an underestimate in X-ray surface flux. Franchini et al. (1988) note that the rotational velocities that they have determined would be over estimated if a substantial veiling flux is present. In Figure 14*a* the data for the Pleiades stars is shown (Stauffer et al. 1993). The Pleiades data can be described as filling a wide band in log F_x at rotational velocities greater than 20 km s^{-1}. Below that velocity much lower values of log F_x can be found. It is difficult to look for a functional relationship in this data since values of v sin i give only lower limits to V_{eq}. However, it is clear that the slowly rotating Pleiades stars exhibit much lower X-ray surface fluxes (Stauffer et al. 1993). The L1495E X-ray data is consistent with the Pleiades data. However, because of the small number of stars in this group having measured v sin i's, only 1 slow rotator, no independent assessment of this behavior can be made for PMS stars from this data. Therefore we cannot separate age and rotation effects.

Because the derivation of other stellar parameters, in particular the stellar mass, are dependent upon the set of stellar evolutionary tracks used, we prefer to wait until the new tracks have been further evaluated until attempting further correlations with derived stellar parameters. It will also be useful to have a larger body of X-ray data derived from the *ROSAT* pointed observations for stellar populations of a range of ages. We will then be able to separate the effects of age and rotation for stars in a small mass range from first appearance to the main sequence.

8. CONCLUSIONS

The L1495E cloud is a region of very active star formation. Our multiwavelength deep survey of this region has considerably increased our knowledge of the PMS population within the cloud. The *ROSAT* PSPC observation allowed us to identify eight new low-mass (0.08 $M_\odot \leq 0.6\ M_\odot$) members of the cloud population. Serendipitous observations of otherwise undistinguished stars has added one (or possibly two) more members. Nearly all of the new members of the cloud population are of spectral type M3 and later and thus represent a heretofore unrepresented fraction of the cloud population. This population appears to be nearly coeval; that is the spread in the H-R diagram is small at any given mass. The mean age lies between 5×10^5 and 1×10^6 yr depending upon the adopted tracks.

These observations combined with the use of "modern" evolutionary tracks allow us to address an outstanding problem concerning the PMS population in the Taurus molecular clouds, the apparent deficiency of stars with masses below $\sim 0.40\ M_\odot$. While the addition of the newly discovered cloud members and the identification of the low-mass companions of other cloud members helps us to alleviate this deficiency, the use of the new evolutionary tracks is the key factor in understanding the mass distribution in the L1495E population. The masses deduced for stars of 1×10^6 yr and younger are considerably lower than those previously derived (Strom et al. 1989b). This allows us to understand the large difference in the effective temperature distribution, as reflected in spectral types, between the PMS population in Lupus and that in Taurus as merely a reflection of different ages of the two groups.

The near-infrared observations of the newly recognized cloud members show that six of eight exhibit colors characteristic of disk emission. With the spectra obtained with HYDRA, we find that, with the possible exception of the serendipitously observed A2 star,

the new cloud members are low-mass stars ($M < 0.6\ M_{\odot}$) and are typically deeply embedded in the cloud. The images of 2 of the low-luminosity *IRAS* sources are extended. These images, in combination with their spectral energy distributions, and the models of Kenyon et al. (1993), demonstrate that these objects are still surrounded by dense core material, even though one of the objects is actually found at the edge of the main cloud.

Although there are only 35 known members of this stellar aggregate, 27 of which lie within the completely sampled region, we show that the observed IMF for this group is consistent with the IMF found by Scalo (1986) for the field population, with a peak near $\log M = -0.5$ and a falloff toward lower masses. There is no evidence for a rise as mass decreases.

The X-ray luminosity of the L1495E stars is highly correlated with the stellar luminosity with a slope to the relationship of 1.80 ± 0.1. This can be seen in the observations of the Cha I stars as well, although the higher mass stars in this group have much lower X-ray luminosities than their counterparts in L1495E, perhaps due to the greater age of the Cha I association ($\sim 2 \times 10^6$ yr on the Alexander tracks). When the X-ray surface flux of the Pleiades sample is examined as a function of the rotational velocity of the stars, it is seen that no systematic variation is found for velocities greater than 20 kms^{-1}. However, below that velocity the range of observed X-ray surface flux increases dramatically with stars of low projected rotational velocities showing the lowest surface fluxes. When the rotational velocity drops below 20 km s^{-1}, the energy source powering the X-ray emission in these stars is substantially diminished. The X-ray data for the L1495E stars is consistent with the Pleiades data. However, there are too few stars in the sample having measured rotational velocities to enable us to separate age and rotation effects.

The authors would like to thank P. Hartigan for obtaining the R and I band CCD frames, and R. Probst, M. Meyer, P. Knezak and L. Hillenbrand for each obtaining part of the near-infrared frames. Without their help this paper would have greatly suffered. The authors would also like to acknowledge support from the National Science Foundation (S. E. S.), the NASA Planetary Science and Origins of Solar Systems programs, the NASA ADP program and, of course, the *ROSAT* observations support (K. M. S.).

APPENDIX

In this section we give the data on the anonymous stars that were serendipitously observed with HYDRA and with SQIID. In Table 5 are given the positions and photometric data for the optically visible stars which are seen projected on the face of the cloud. Five of these stars are discussed in the text.

In Table 6 are given approximate positions and near-infrared photometric data for stars appearing in our SQIID frames whose colors indicate that they might be cloud members.

TABLE 5

ANONYMOUS SOURCES IN THE *ROSAT* FIELD

Object	α(1950)	δ(1950)	R	I	R-I	J	H	K	J-H	H-K
Anon 1	4 15 24.49	28 10 15	18.26 ± 0.16	16.67 ± 0.03	1.59	14.56 ± 0.21	14.65 ± 0.28	13.72 ± 0.25	-0.09	0.93
Anon 2	4 15 24.95	28 11 12	18.62 ± 0.22	16.94 ± 0.04	1.68	14.43 ± 0.17	13.17 ± 0.08	12.46 ± 0.07	1.26	0.71
Anon 3	4 15 20.84	28 12 55	17.31 ± 0.07	15.45 ± 0.01	1.86					
Anon 4	4 15 17.10	28 09 51	16.86 ± 0.04	15.50 ± 0.01	1.36					
Anon 5	4 15 24.02	28 08 55	...	17.63 ± 0.10	...					
Anon 6	4 15 24.38	28 08 30	...	18.97 ± 0.26	...					
Anon 7	4 15 54.62	28 17 29	18.67 ± 0.22	17.03 ± 0.04	1.64					
Anon 8	4 15 52.03	28 19 33	18.19 ± 0.15	16.71 ± 0.03	1.48					
Anon 9	4 15 39.20	28 19 27	15.49 ± 0.01	13.28 ± 0.01	2.10	10.15 ± 0.04	8.84 ± 0.05	7.96 ± 0.04	1.31	0.88
Anon 10	4 15 47.96	28 19 12	19.82 ± 0.65	18.34 ± 0.13	1.5:					
Anon 11	4 15 43.81	28 20 35	> 20	17.85 ± 0.09	> 2.2					
Anon 12	4 15 10.19	28 20 42	14.94 ± 0.01	13.29 ± 0.01	1.66	12.18 ± 0.01	11.63 ± 0.01	11.36 ± 0.01	0.55	0.27
Anon 13	4 15 10.95	28 21 27	18.58 ± 0.20	15.97 ± 0.02	2.61	12.82 ± 0.04	11.64 ± 0.05	10.90 ± 0.04	1.18	0.74
Anon 14	4 14 59.26	28 20 45	17.85 ± 0.11	15.80 ± 0.01	2.06					
Anon 15	4 15 00.80	28 22 39	20.4:	17.67 ± 0.07	~ 2.7					
Anon 16	4 15 03.67	28 04 04	19.36 ± 0.42	17.87 ± 0.09	1.49					
Anon 17	4 14 59.71	28 14 50	13.81 ± 0.04	12.76 ± 0.01	1.05					
Anon 18	4 15 05.25	28 11 42	18.74 ± 0.24	16.89 ± 0.04	1.85					
Anon 19	4 15 06.53	28 12 22	18.60 ± 0.21	17.13 ± 0.04	1.46					

TABLE 6

ANONYMOUS SOURCES IN THE NEAR-INFRARED FRAMES

Object	α(1950)	δ(1950)	J	H	K	J-H	H-K
Anon 20	4 15 39.11	28 13 40	...	13.58 ± 0.10	11.92 ± 0.04	...	1.66
Anon 21	4 15 40.69	28 13 30	...	13.71 ± 0.13	12.39 ± 0.06	...	1.32
Anon 22	4 14 54.27	28 20 38	16.27 ± 0.20	15.62 ± 0.30	14.75 ± 0.25	0.65	0.87
Anon 23	4 15 01.31	28 16 18	15.42 ± 0.10	15.83 ± 0.3	14.34 ± 0.15	0.39	1.49
Anon 24	4 15 16.16	28 17 17	14.84 ± 0.05	12.27 ± 0.10	10.65 ± 0.01	2.57	1.62
Anon 25	4 15 23.76	28 18 58	14.75 ± 0.10	11.73 ± 0.02	9.88 ± 0.01	3.02	1.85
Anon 26	4 15 29.93	28 19 03	...	16.44 ± 0.40	13.30 ± 0.10	...	3.11
Anon 27	4 15 31.66	28 17 59	...	15.60 ± 0.30	13.50 ± 0.10	...	2.10

REFERENCES

Appenzeller, I., Jankovics, I., & Krautter, J. 1983, A&AS, 53, 291
Bahcall, J. N., & Soneira, R. M. 1980, ApJS, 44, 73
Barsony, M., & Kenyon, S. J. 1992, ApJ, 384, L53
Beichman, C. A., Boulanger, F., & Moshir, M. 1992, ApJ, 386, 248
Bertout, C., Basri, G., & Bouvier, J. 1988, ApJ, 330, 350
Bessell, M. S., & Brett, J. M. 1988, PASP, 100, 1134
Bouvier, J. 1990, AJ, 99, 946
Bouvier, J., & Bertout, C. 1989, A&A, 211, 99
Bouvier, J., Bertout, C., Benz, W., & Mayor, M. 1986, A&A, 165, 110
Bouvier, J., Cabrit, S., Fernández, M., Martín, E. L., & Matthews, J. M. 1993, A&A, 272, 176
Briceño, C., Calvet, N., Gomez, M., Hartmann, L., Kenyon, S., & Whitney, B. 1993, PASP, 105, 686
Caillault, J.-P., & Zoonematkermani, S. 1989, ApJ, 338, L57
Cohen, M., & Kuhi, L. V. 1979, ApJS, 41, 743
D'Antona, F., & Mazzitelli, I. 1994, ApJS, 90, 861
Davis, L. 1993 in ASP Conf. Ser. 52, Astronomical Data Analysis Software and Systems II, ed. R. J. Hanish, R. J. V. Brissenden & J. Barnes (San Francisco: ASP), 52
Duvert, G., Cernicharo, J., & Baudry, A. 1986, A&A, 164, 349
Edwards, S., et al. 1993, AJ, 106, 372
Feigelson, E. D. 1986 in Protostars and Molecular Clouds, ed. T. Montmerle & C. Bertout (Saclay: Centre d'Etudes Nucleaire de Saclay), 123
Feigelson, E. D., Casanova, S., Montmerle, T., & Guibert, J. 1993, ApJ, 416, 623
Feigelson, E. D., & DeCampli, W. M. 1981, ApJ, 243, L89
Feigelson, E. D., & Kriss, G. A. 1989, ApJ, 338, 262
Franchini, M., Magazzú, A., & Stalio, R. 1988, A&A, 189, 132; errata 197, 354
Fukui, Y., Mizuno, A., Nagahama, T., Imaoka, K., & Ogawa, H. 1991, Mem. Soc. Astron. Ital., 62, 301
Gauvin, L. S., & Strom, K. M. 1992, ApJ, 385, 217
Ghez, A. 1993, Ph.D. thesis, California Inst. of Technology
Ghez, A., Neugebauer, G., & Matthews, K. 1992, in IAU Colloq. 135, Complementary Approaches to Double and Multiple Star Research, ed. H. A. McAlister & W. I. Hartkopf (San Francisco: ASP), 1
Gomez, M., Jones, B. F., Hartmann, L. W., Kenyon, S. J., Stauffer, J. R., Hewett, R., & Reid, N. 1992, AJ, 104, 762
Goodrich, R. W. 1993, ApJS, 86, 499
Hartigan, P. 1993, AJ, 105, 1511
Hartigan, P., Kenyon, S. J., Hartmann, L. W., Strom, S. E., Edwards, S., Welty, A. D., & Stauffer, J. 1992, ApJ, 382, 617
Hartigan, P., Strom, K. M., & Strom, S. E. 1994, ApJ, in press
Hartmann, L. W., Hewett, R., Stahler, S., & Mathieu, R. D. 1986, ApJ, 309, 275
Hartmann, L. W., Jones, B. F., Stauffer, J. R., & Kenyon, S. J. 1991, AJ, 101, 1050
Hartmann, L. W., Kenyon, S. J., & Hartigan, P. 1993, in Protostars and Planets III, ed. E. H. Levy & J. I. Lunine (Tucson: Univ. Arizona Press)
Hartmann, L. W., & Stauffer, J. R. 1989, AJ, 97, 873
Herbig, G. H., & Bell, K. R. 1988, Lick Obs. Bull. Ser., No. 1111
Herbig, G. H., Vrba, F. J., & Rydgren, A. E. 1986, AJ, 91, 575
Hughes, J., & Hartigan, P. 1992, AJ, 104, 680
Jones, B. F., & Herbig, G.H. 1979, AJ, 84, 1872
Jones, B. F., & Stauffer, J. R. 1991, AJ, 102, 1080
Kenyon, S. J., Calvet, N., & Hartmann, L. 1993a, ApJ, 414, 676
Kenyon, S. J., Whitney, B. A., Gomez, M., & Hartmann, L. 1993b, ApJ, 414, 773
Kim, Ch. Y. 1990, in Mem. Kyoto Univ. Ser. Phys., Astrophys. Geophys. Chem., Vol. 38, No. 1, Art. 1
Kirkpatrick, J. D., Henry, T. J., & McCarthy, D. W., Jr. 1991, ApJS, 77, 417
Kroupa, P., Tout, C. A., & Gilmore, G. 1990, MNRAS, 244, 76
Krautter, J., & Kelemen, J. 1987, Mitt. Astron. Ges., 70, 397
Lada, C. J. 1987, in IAU Symp. 115, Star-Forming Regions, ed. M. Peimbert & J. Jugaku (Dordrecht: Reidel), 1
Lada, C. J., Margulis, M., & Dearborn, D. 1984, ApJ, 285, 141
Landolt, A. U. 1992, AJ, 104, 304
Leinert, Ch., et al. 1992, in IAU Colloq. 135, Complementary Approaches to Double and Multiple Star Research, ed. H. A. McAlister & W. I. Hartkopf (San Francisco: ASP), 21
Montmerle, T., Koch-Miramond, L., Falgerone, E., & Grindlay, J. E. 1983, ApJ, 269, 182
Morrison, R., & McCammon, D. 1983, ApJ, 270, 119
Ohnishi, T., & Mizuno, A. 1993, private communication
Pravdo, S. H., & Angelini, L. 1993, ApJ, 407, 232
Pfefferman, E., et al. 1986, Proc. SPIE, 773, 519
Raymond, J. C., & Smith, B. W. 1977, ApJS, 35, 419
Reipurth, B., & Zinnecker, H. 1993, A&A, in press
Rosner, R. 1980, in Smithsonian Astrophys. Obs. Spec. Rep., No. 389, 79
Rydgren, A. E., Zak, D. S., Vrba, F. J., Chugainov, P. F., & Zajtseva, G. V. 1984, AJ, 89, 1015
Scalo, J. 1986, Fund. Cosmic Phys., 11, 1
Schmidt-Kaler, T. H. 1982, in Landolt-Bornstein New Ser., Vol. 2b, Astronomy and Astrophysics—Stars and Star Clusters, ed. K. Shaifers & H. H. Voigt (New York: Springer), 1
Schmitt, J. H. M. M., Golub, L., Harnden, F. R., Jr., Maxon, C. W., Rosner, R., & Vaiana, G. S. 1985, ApJ, 290, 307
Schrijver, C. J., Lemen, J. R., & Mewe, R. 1989, ApJ, 341, 484
Schwartz, R. D. 1977, ApJS, 35, 161
Simon, M. 1992, in IAU Colloq. 135, Complementary Approaches to Double and Multiple Star Research, ed. H. A. McAlister & W. I. Hartkopf (San Francisco: ASP), 41
Simon, M., Chen, W. P., Howell, R. R., Benson, J. A., & Slowik, D. 1992, ApJ, 384, 212
Skinner, S. L. 1993, ApJ, 408, 660
Skinner, S. L., Brown, A., & Stewart, R. T. 1993, ApJS, 87, 217
Skrutskie, M. F., Meyer, M. R., & Coutu, R. 1994, in preparation
Stauffer, J. R., Caillault, J.-P., Gagné, M., Prosser, C. F., & Hartmann, L. W. 1994, ApJ, submitted
Strom, K. M., Strom, S. E., Edwards, S., Cabrit, S., & Skrutskie, M. F. 1989b, AJ, 97, 1451
Strom, K. M., Strom, S. E., & Merrill, K. M. 1993, ApJ, 412, 233
Strom, K. M., Strom, S. E., Morgan, J., & Wolff, S. 1986, ApJS, 62, 39
Strom, K. M., et al. 1990, ApJ, 362, 168
Strom, K. M., Wilkin, F. P., Strom, S. E., & Seaman, R. L. 1989a, AJ, 98, 1444
Swenson, F. J., Faulkner, J., Rogers, F. J., & Iglesias, C. A. 1994, ApJ, submitted
Thornley, M., Woodward, C. E., Pipher, J. L., Forrest, W. J., Sellgren, K., & Shure, M. A. 1989, BAAS, 21, 1085
Tinney, C. G., Mould, J. R., & Reid, I. N. 1992, ApJ, 396, 173
Trümper, J. 1983, Adv. Space Res., 2, 241
Tufte, E. R. 1983, The Visual Display of Quantitative Information (Cheshire, CT: Graphics)
Vrba, F. J., Rydgren, A. E., Chugainov, P. F., Shakovskaya, N. I., & Weaver, W. B. 1988, AJ, 97, 483
Vrba, F. J., Rydgren, A. E., Chugainov, P. F., Shakovskaya, N. I., & Zak, D. S. 1986, ApJ, 306, 199
Walter, F. M. 1992, AJ, 104, 758
Walter, F. M., Brown, A., Mathieu, R. D., Myers, P. C., & Vrba, F. J. 1988, AJ, 96, 297